



UNIVERSITÀ
DEGLI STUDI
DI PADOVA



Lifetime Measurements in the $N = 126$ Region with the Reversed Plunger Configuration

D. Brugnara^a, M. Sedlak^b, J. Pellumaj^{c,d}, B. Gongora-Servin^{c,d}
J. J. Valiente Dobón^e,

^aINFN Laboratori Nazionali di Legnaro, Legnaro, Italy

^bInstitute of Physics, Slovak Academy of Science, Bratislava, Slovakia

^cUniversità degli Studi di Padova, Padova, Italy

^dINFN Sezione di Padova, Padova, Italy

^eIFIC, Valencia, Spain



Outline



Aim



Scientific motivation



Reversed Plunger



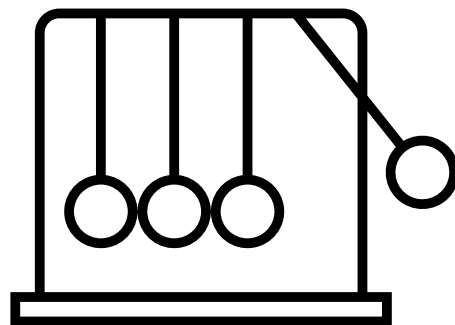
Analysis

- PRISMA Analysis
- γ -ray spectroscopy



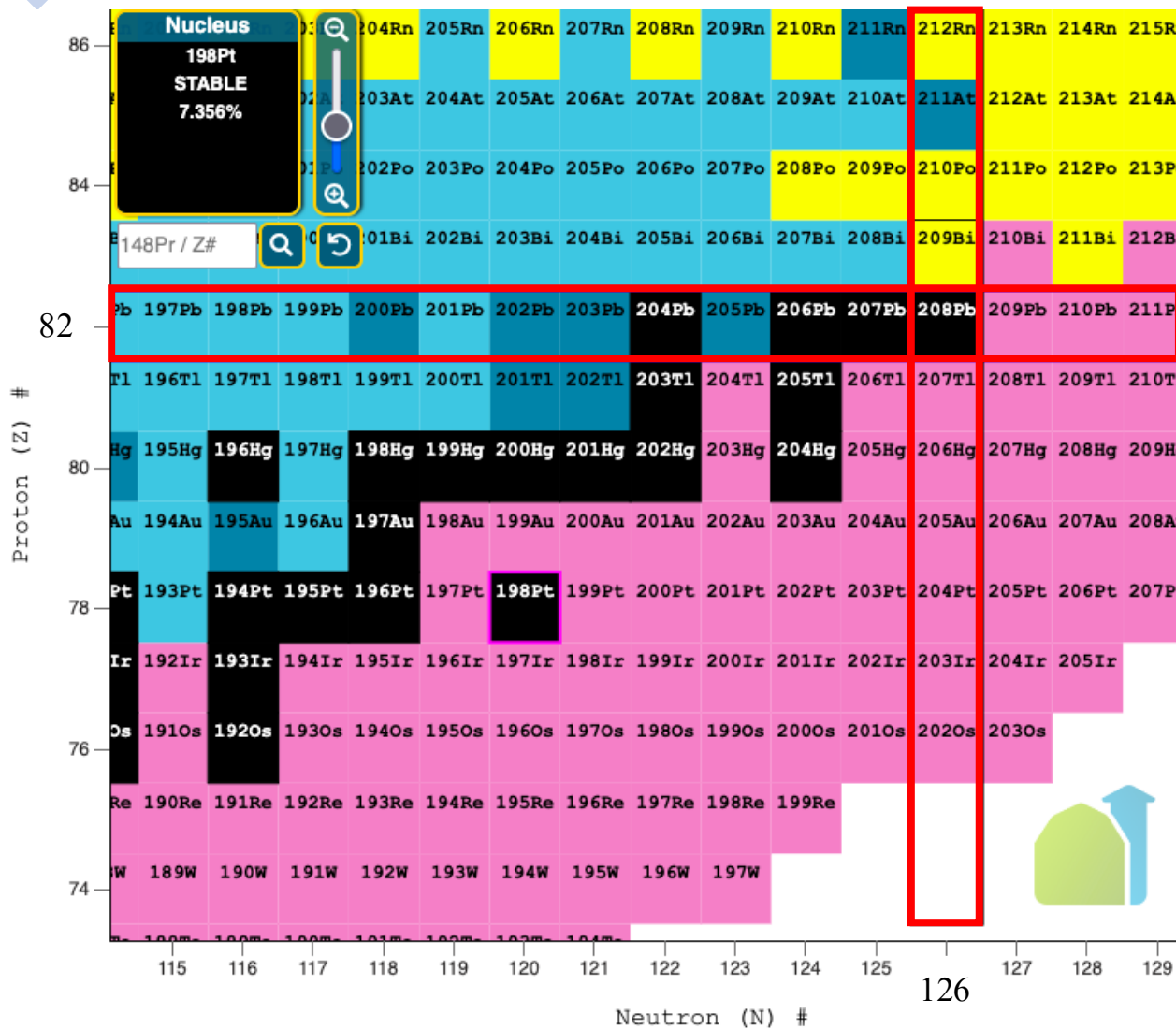
Aim

Study the nuclear shape evolution towards the $N = 126$ shell closure via lifetime measurements of the low-lying states of the neutron-rich nuclei in the vicinity of the stable ^{198}Pt using the plunger device in the reversed configuration

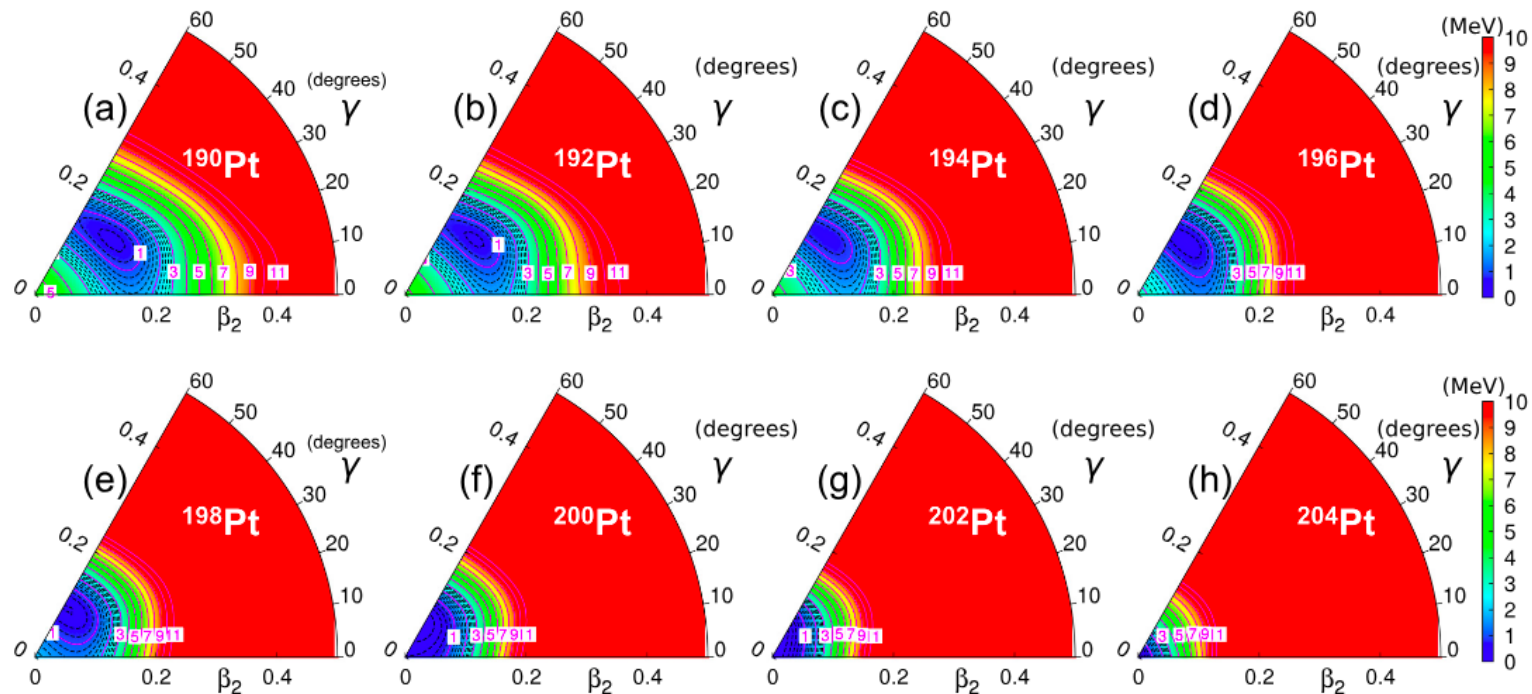


Shape Evolution in Neutron-rich Pt – Os Even-Even Isotopes

Neutron-rich nuclei towards $N=126$



Neutron-rich platinum isotopes are an excellent set to study shape evolution towards the $N = 126$ shell closure

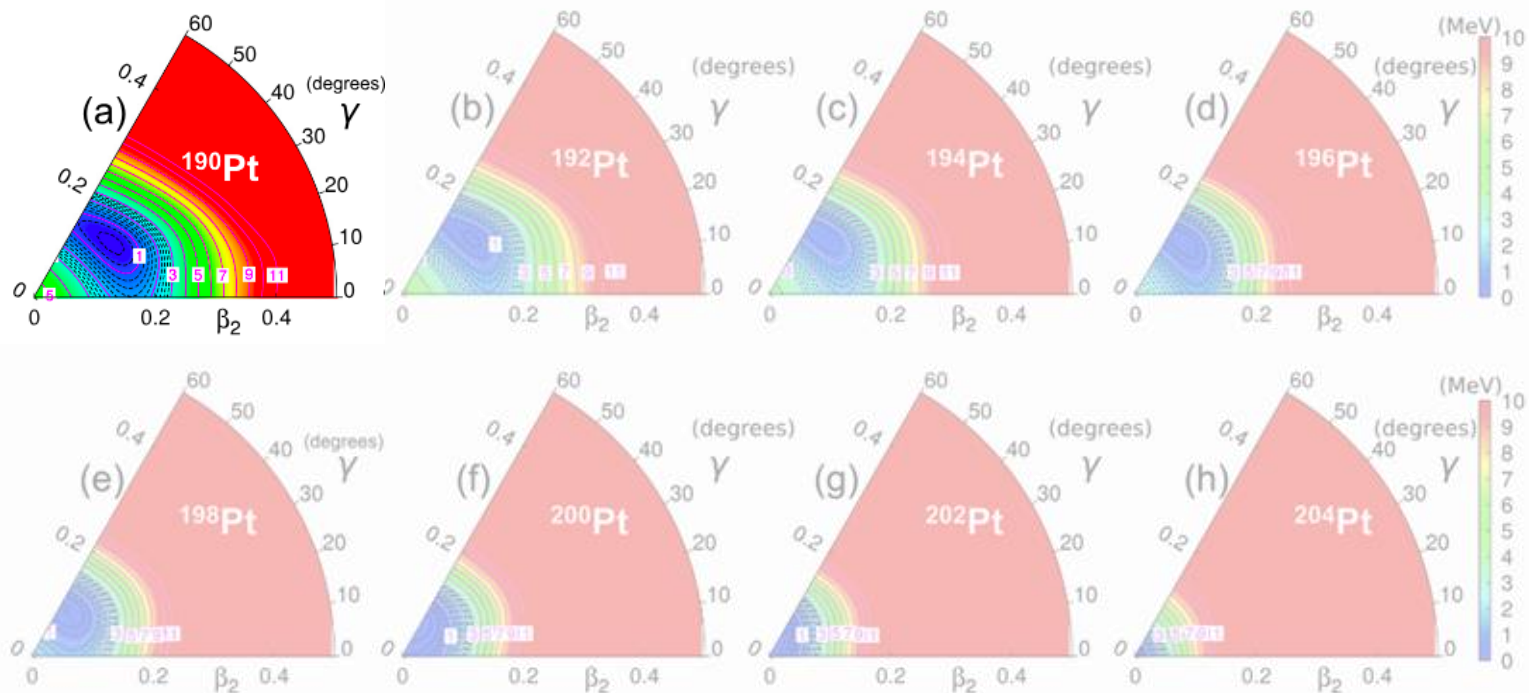


Particle-number-projected potential energy surfaces (PES) in the triaxial plane for $^{190-204}\text{Pt}$ isotopes calculated with the Gogny D1S interaction.

PRC 95, 064321 (2017)

Platinum

Triaxial deformed shape
 $(\beta_2, \gamma) \approx (0.15, 40^\circ)$



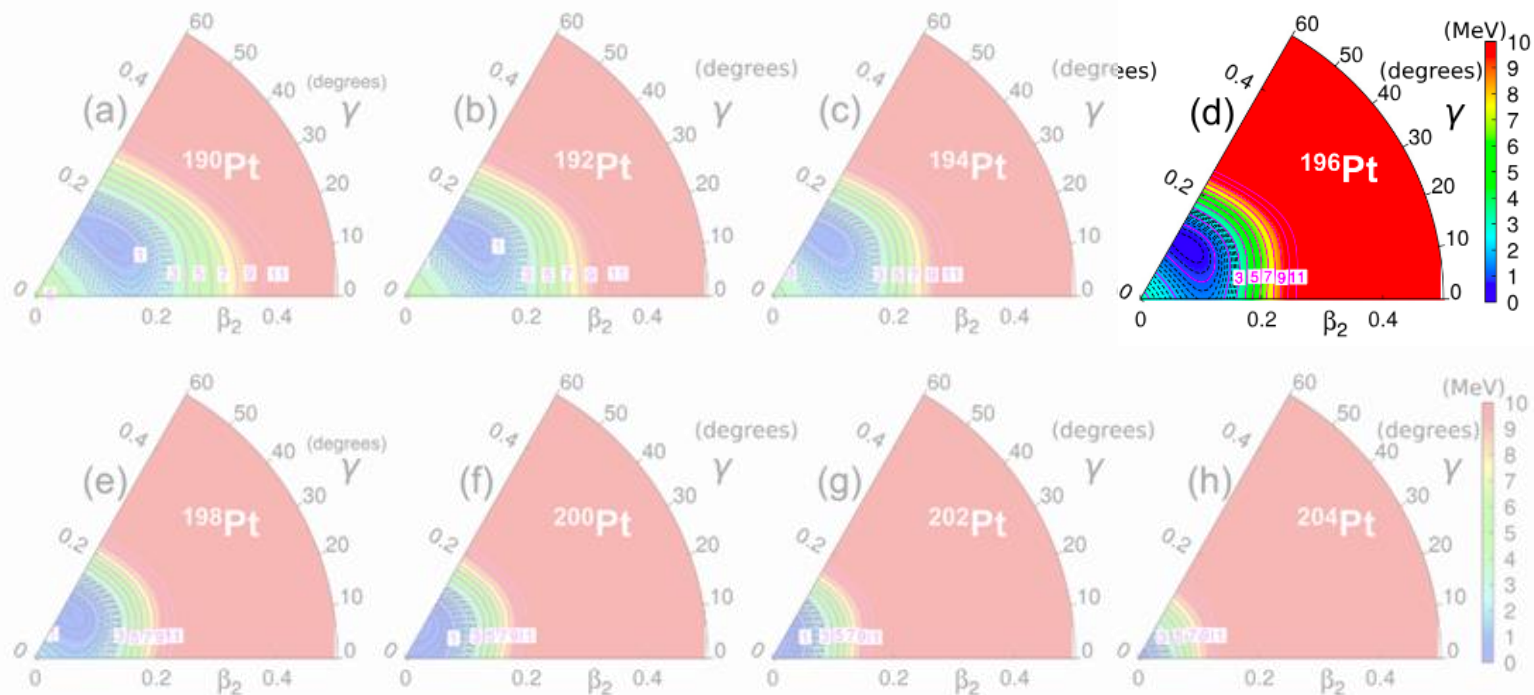
Particle-number-projected potential energy surfaces (PES) in the triaxial plane for $^{190-204}\text{Pt}$ isotopes calculated with the Gogny D1S interaction.

PRC 95, 064321 (2017)

Platinum

Triaxial deformed shape
 $(\beta_2, \gamma) \approx (0.15, 40^\circ)$

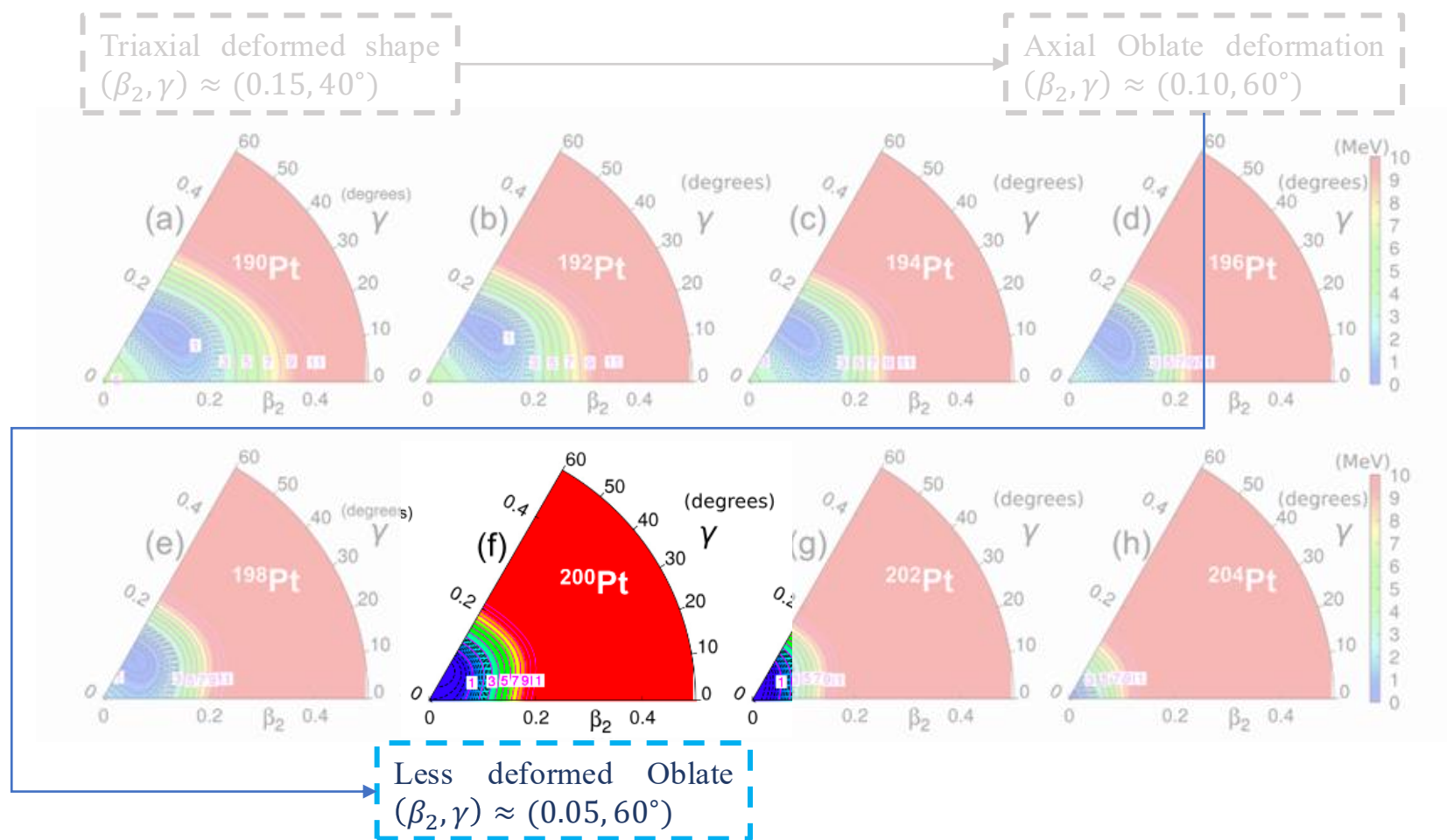
Axial Oblate deformation
 $(\beta_2, \gamma) \approx (0.10, 60^\circ)$



Particle-number-projected potential energy surfaces (PES) in the triaxial plane for $^{190-204}\text{Pt}$ isotopes calculated with the Gogny D1S interaction.

PRC 95, 064321 (2017)

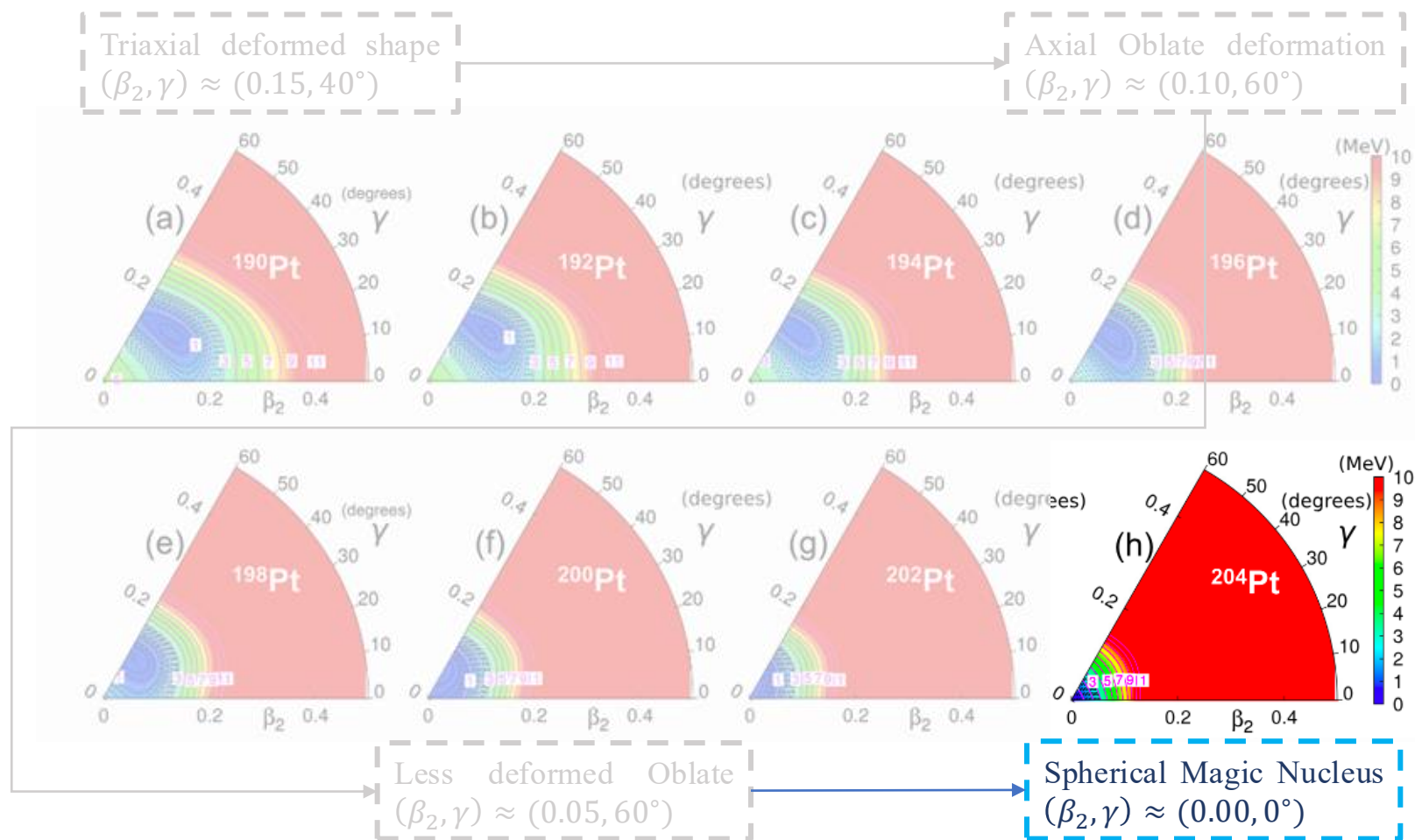
Platinum



Particle-number-projected potential energy surfaces (PES) in the triaxial plane for $^{190-204}\text{Pt}$ isotopes calculated with the Gogny D1S interaction.

PRC 95, 064321 (2017)

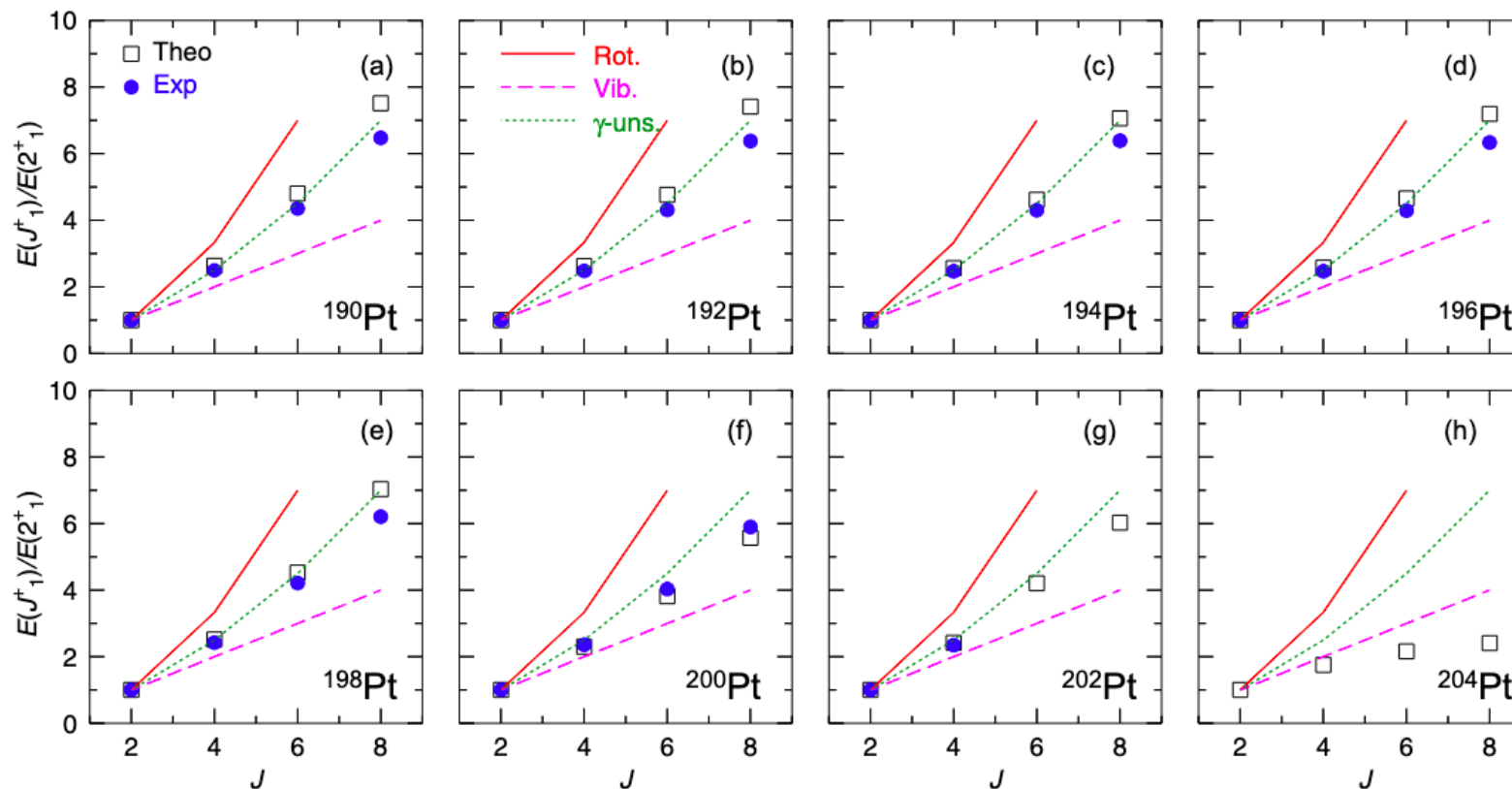
Platinum



Particle-number-projected potential energy surfaces (PES) in the triaxial plane for $^{190-204}\text{Pt}$ isotopes calculated with the Gogny D1S interaction.

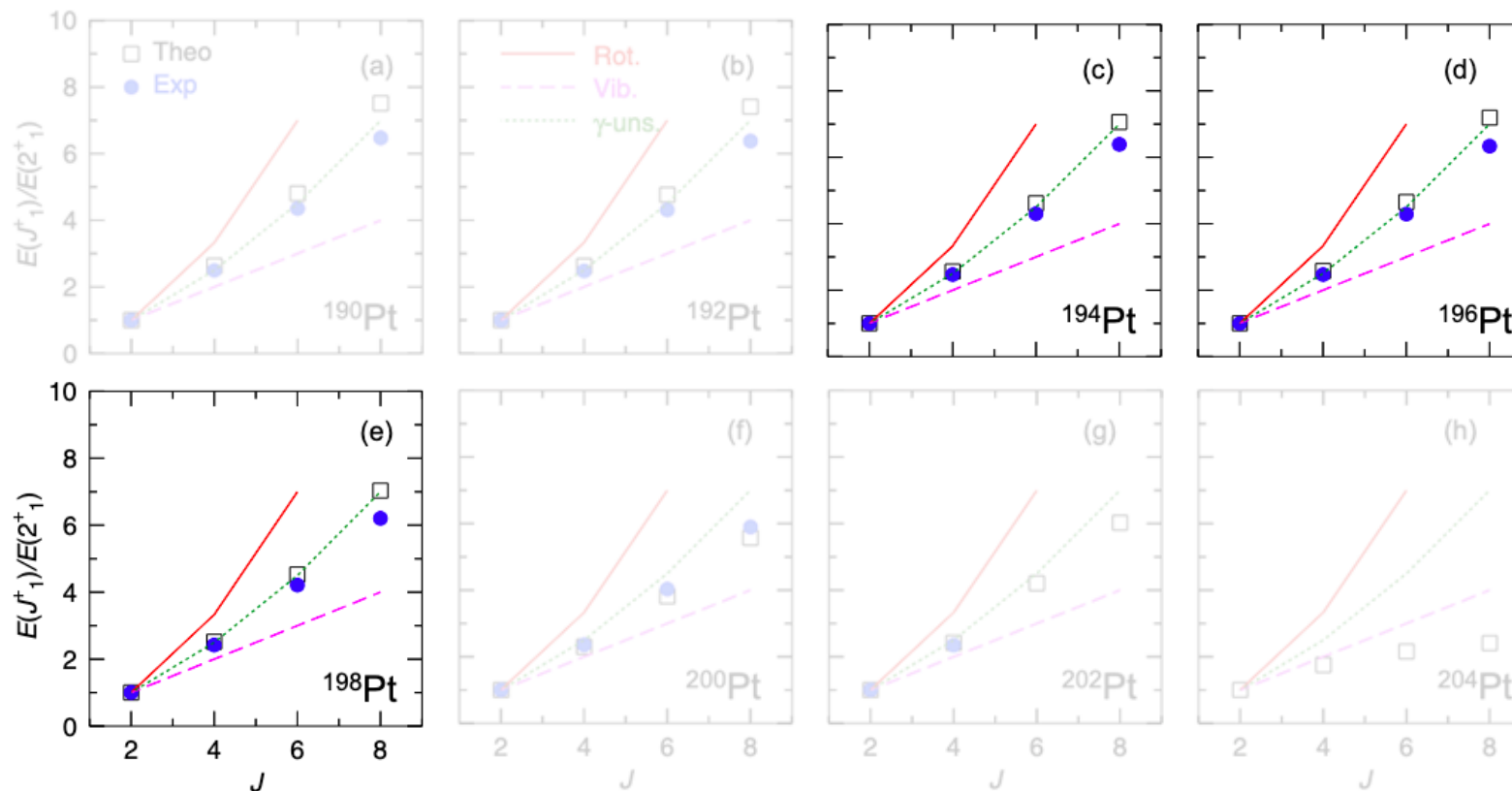
PRC 95, 064321 (2017)

Platinum



Yrast band excitation energies, normalized to the corresponding 2_1^+ energies, for $^{190-204}\text{Pt}$ isotopes. Blue dots and black boxes are the experimental points and theoretical beyond-mean-field predictions, respectively.

Platinum

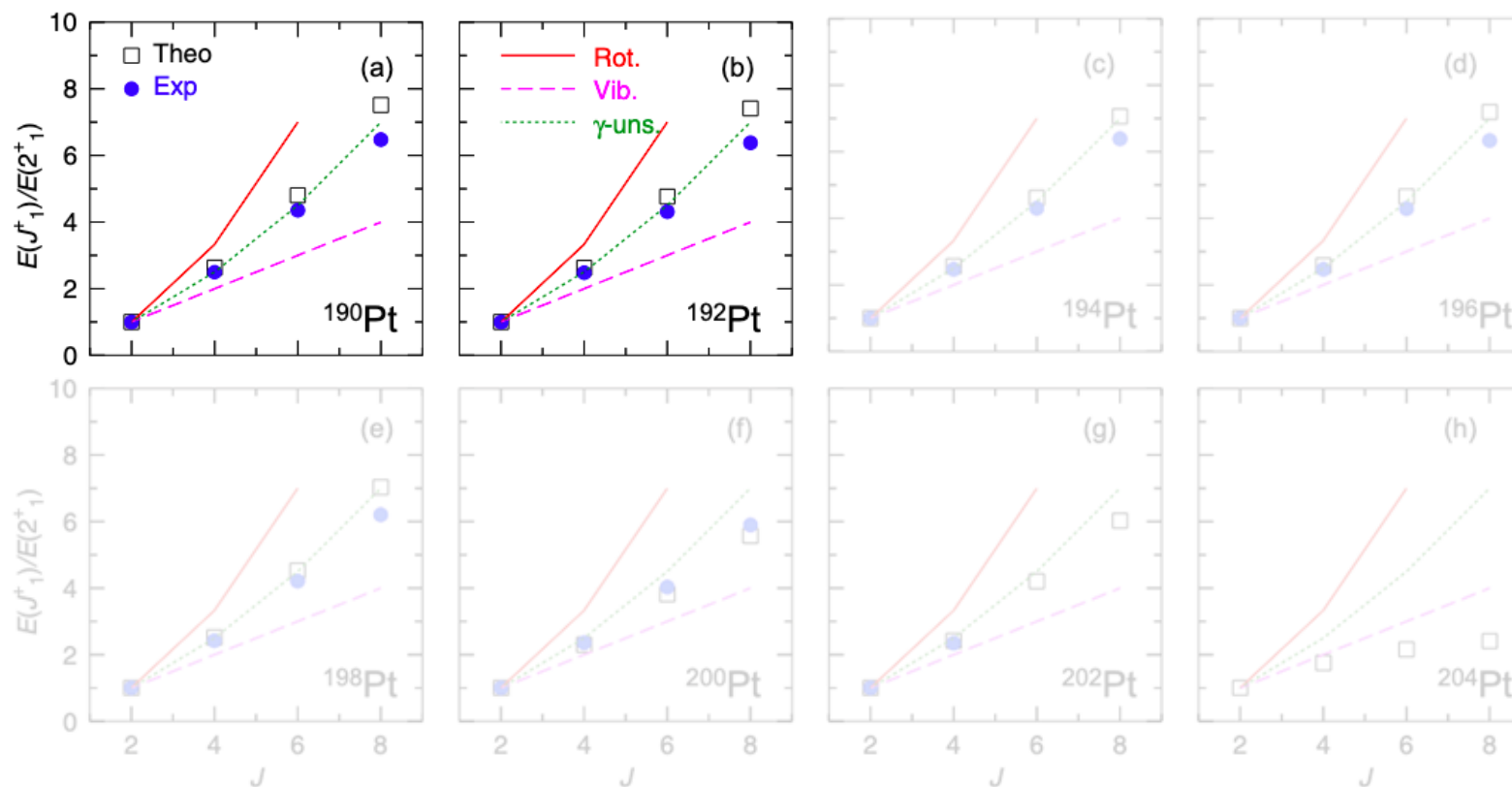


γ -unstable/triaxial rotor
geometrical model
reproduces the
experimental data with
good agreement

Yrast band excitation energies, normalized to the corresponding 2_1^+ energies, for $^{190-204}\text{Pt}$ isotopes. Blue dots and black boxes are the experimental points and theoretical beyond-mean-field predictions, respectively.

Platinum

Tiny deviations
towards a more
axial rotational
character



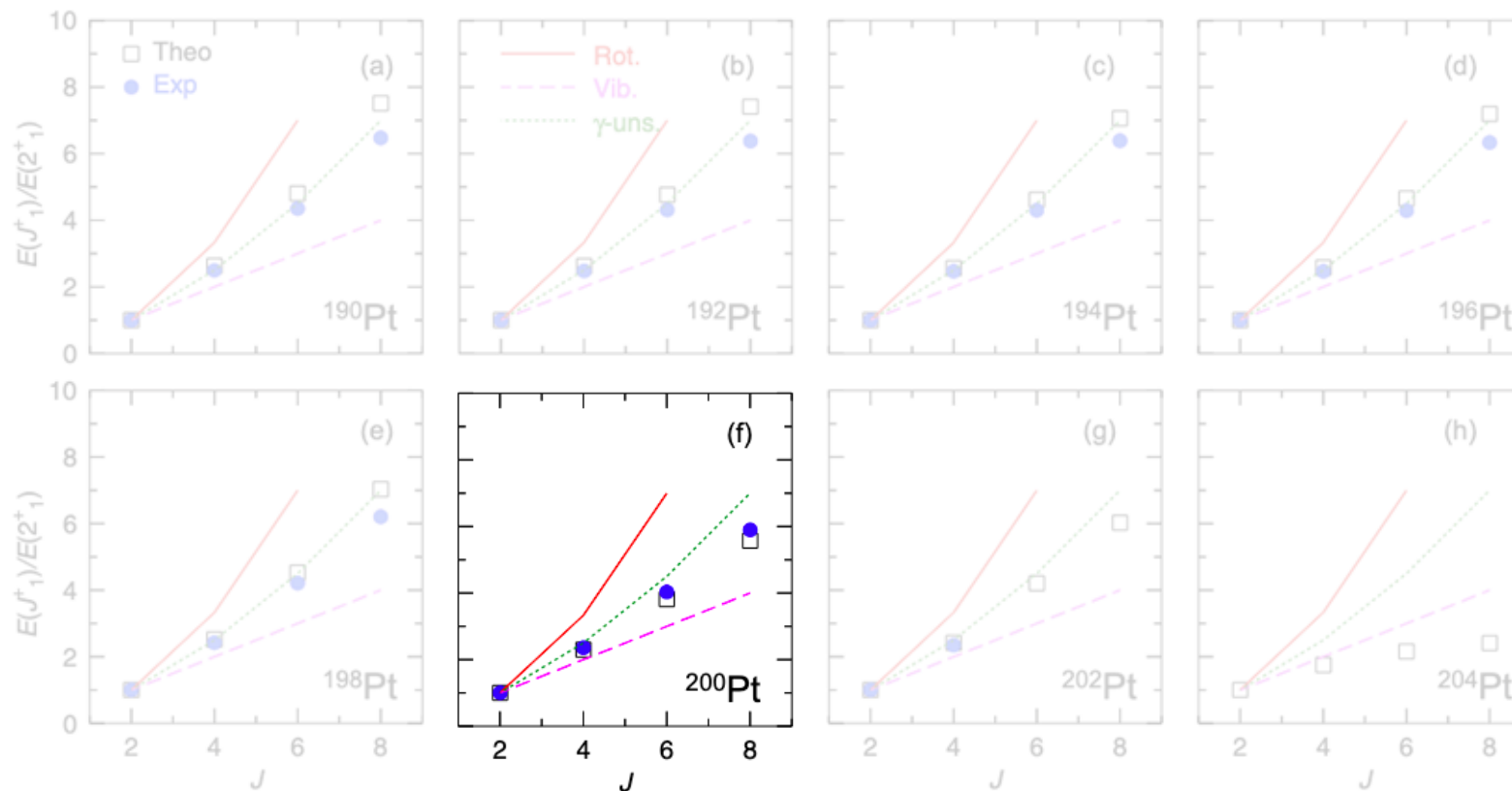
γ -unstable/triaxial rotor
geometrical model
reproduces the
experimental data with
good agreement

Yrast band excitation energies, normalized to the corresponding 2_1^+ energies, for $^{190-204}\text{Pt}$ isotopes. Blue dots and black boxes are the experimental points and theoretical beyond-mean-field predictions, respectively.

Platinum

Tiny deviations
towards a more
axial rotational
character

Tiny deviations
towards a more
vibrational
character

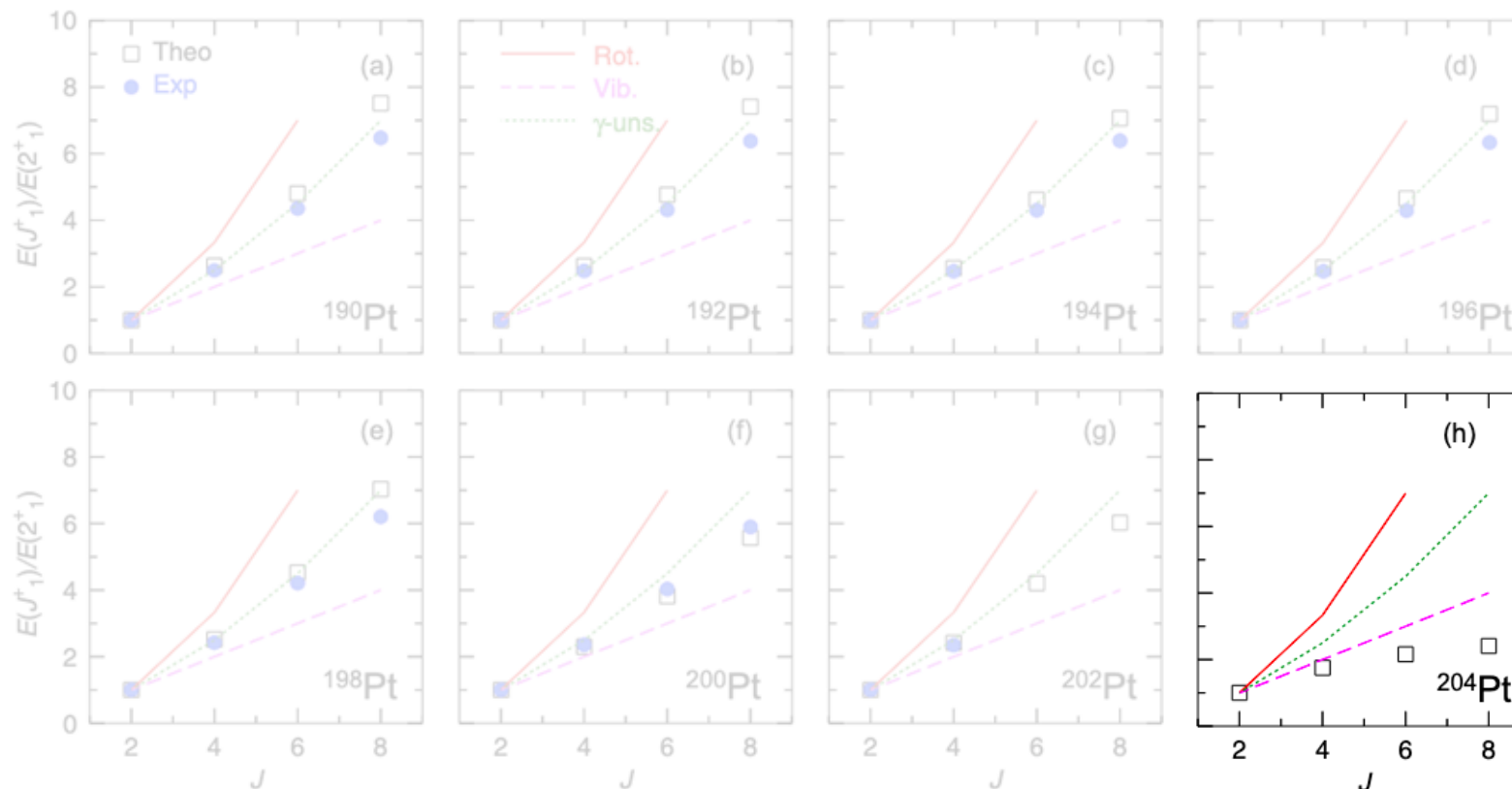


γ -unstable/triaxial rotor
geometrical model
reproduces the
experimental data with
good agreement

Yrast band excitation energies, normalized to the corresponding 2_1^+ energies, for $^{190-204}\text{Pt}$ isotopes. Blue dots and black boxes are the experimental points and theoretical beyond-mean-field predictions, respectively.

Platinum

Tiny deviations
towards a more
axial rotational
character



γ -unstable/triaxial rotor
geometrical model
reproduces the
experimental data with
good agreement

Tiny deviations
towards a more
vibrational
character

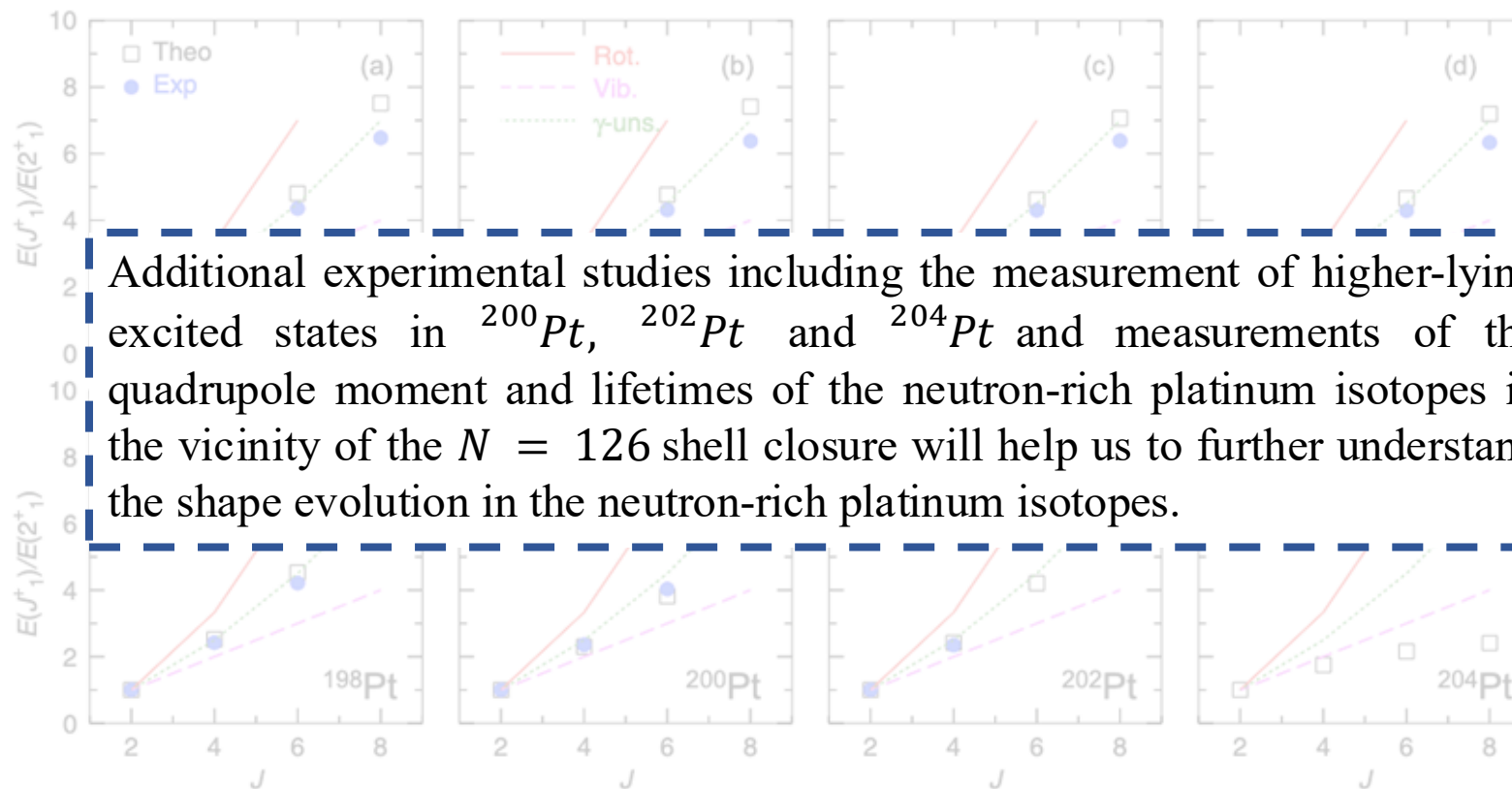
Purely spherical, and
the excited states go
even below the
vibrational limit

Yrast band excitation energies, normalized to the corresponding 2_1^+ energies, for $^{190-204}\text{Pt}$ isotopes. Blue dots and black boxes are the experimental points and theoretical beyond-mean-field predictions, respectively.

Platinum

Tiny deviations towards a more axial rotational character

Tiny deviations towards a more vibrational character



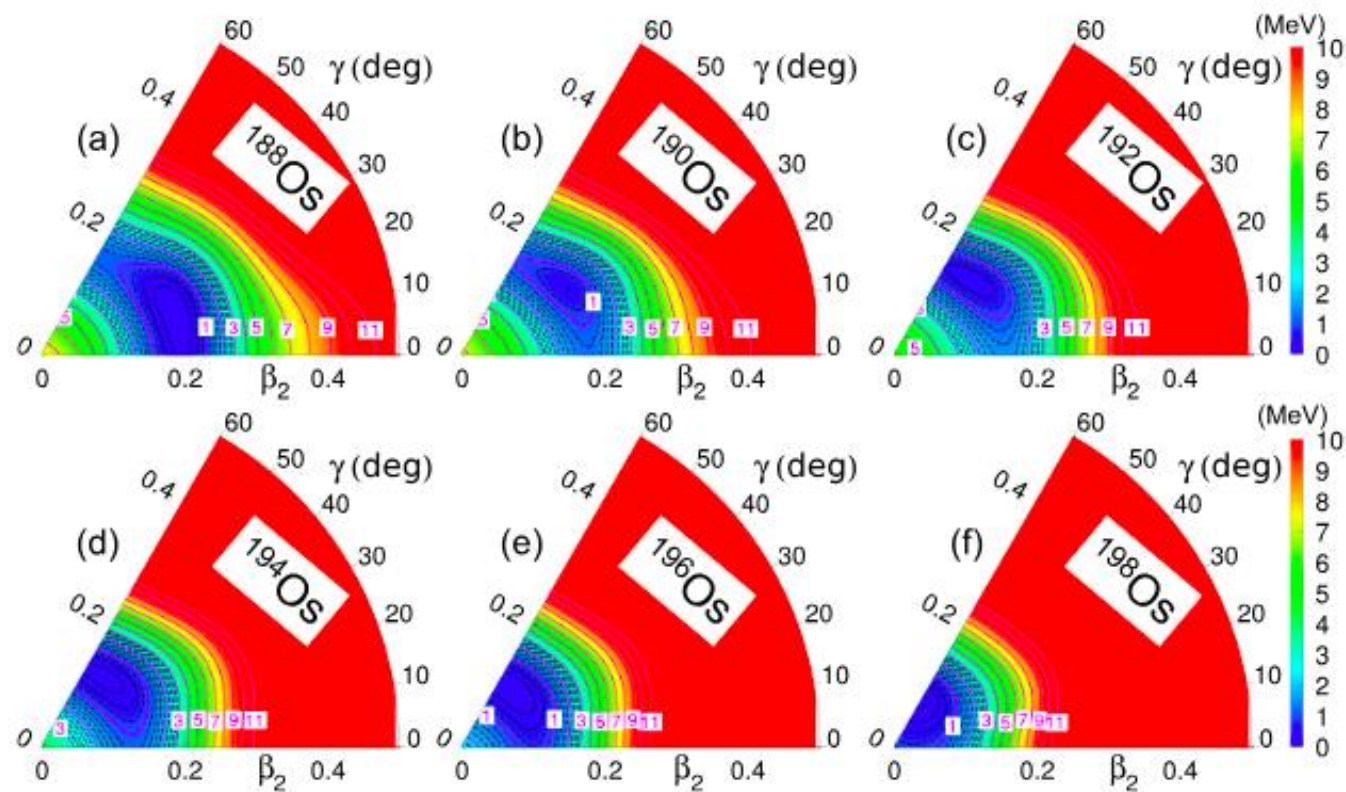
Additional experimental studies including the measurement of higher-lying excited states in ^{200}Pt , ^{202}Pt and ^{204}Pt and measurements of the quadrupole moment and lifetimes of the neutron-rich platinum isotopes in the vicinity of the $N = 126$ shell closure will help us to further understand the shape evolution in the neutron-rich platinum isotopes.

γ -unstable/triaxial rotor geometrical model reproduces the experimental data with good agreement

Purely spherical, and the excited states go even below the vibrational limit

Yrast band excitation energies, normalized to the corresponding 2_1^+ energies, for $^{190-204}\text{Pt}$ isotopes. Blue dots and black boxes are the experimental points and theoretical beyond-mean-field predictions, respectively.

Osmium

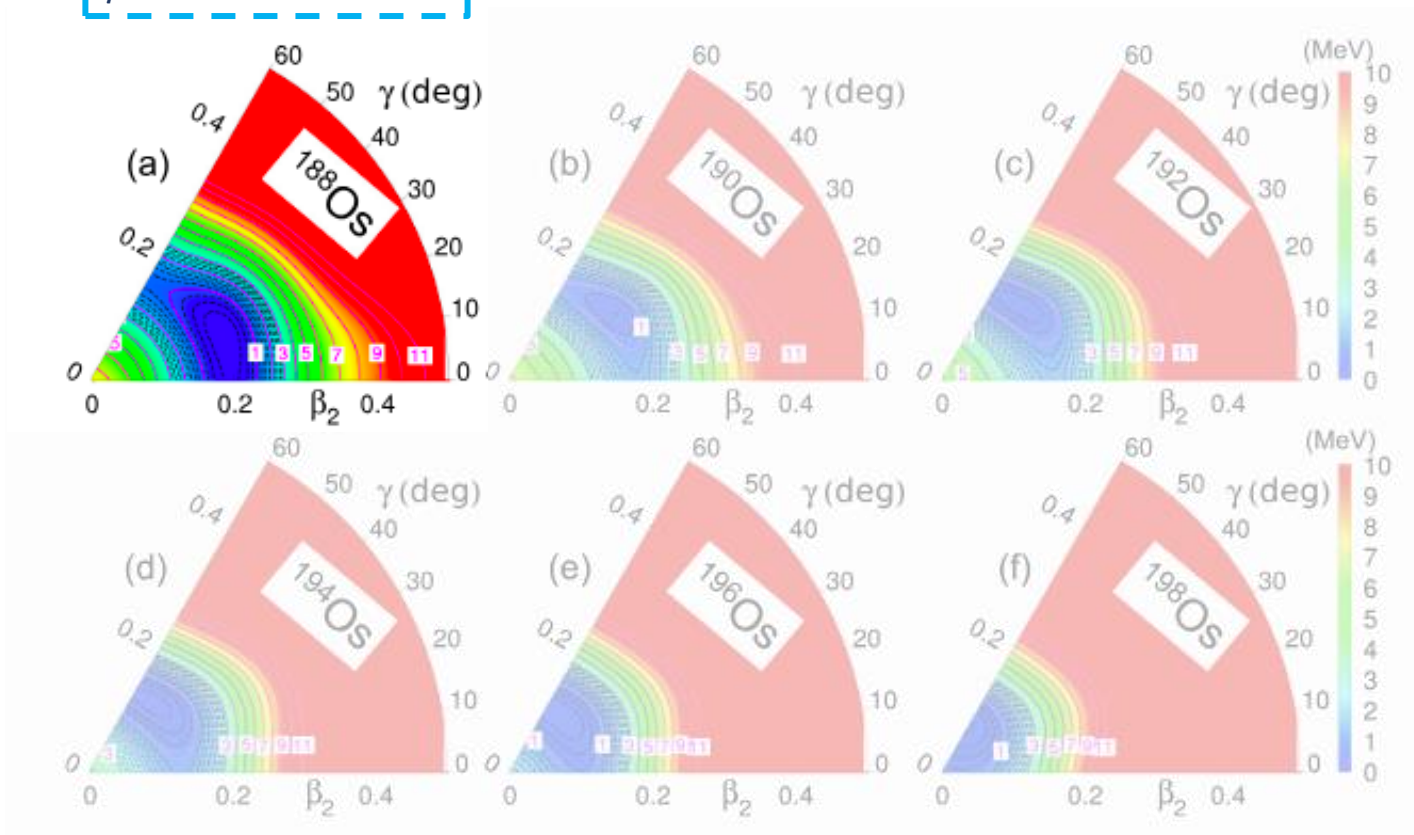


Particle number projected potential energy surfaces in the triaxial plane for $^{188-198}\text{Os}$ isotopes calculated with the Gogny D1S interaction.

PRC 90, 021301(R) (2014)

Osmium

Prolate deformation
 $\gamma \approx 0^\circ$

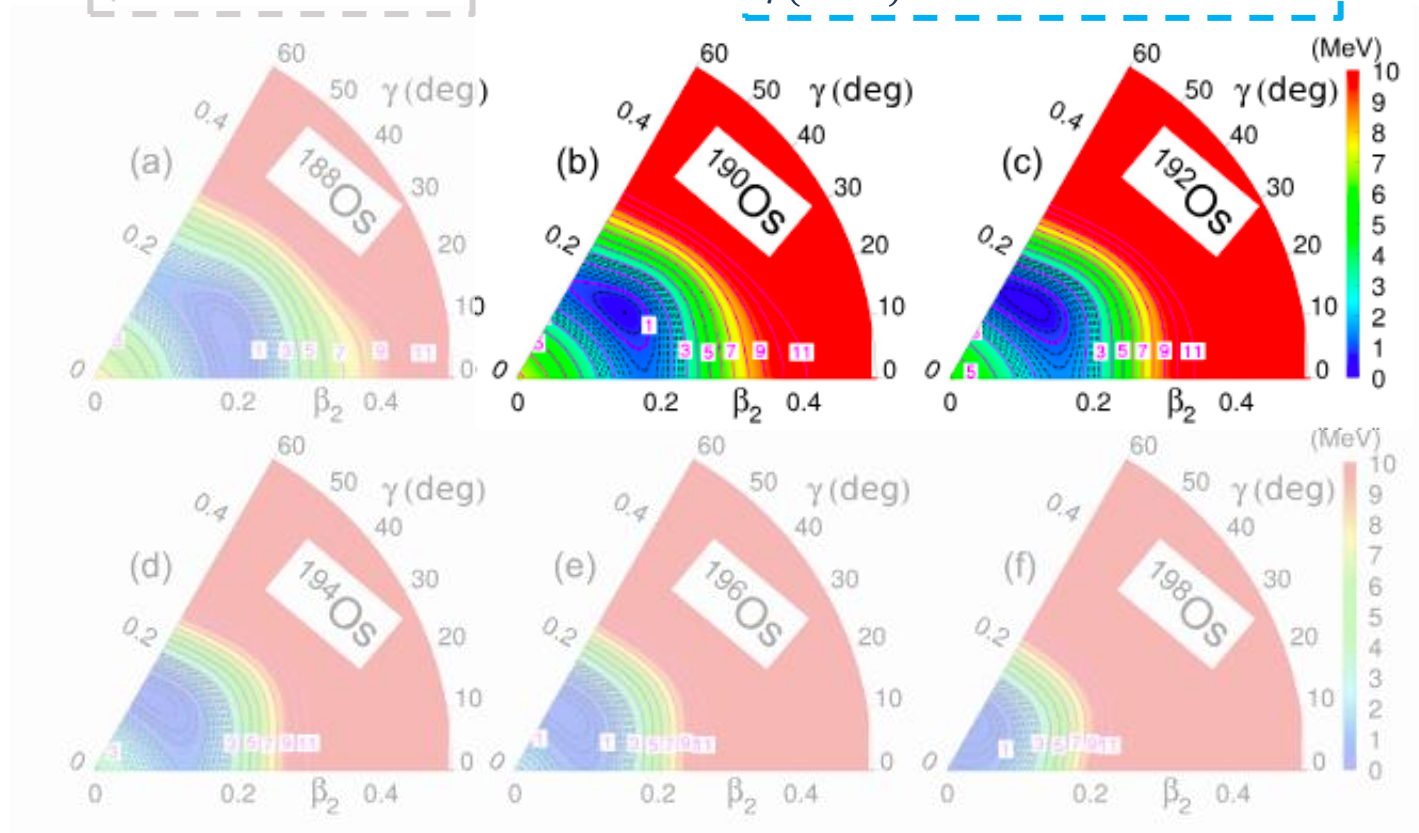


Particle number projected potential energy surfaces in the triaxial plane for $^{188-198}\text{Os}$ isotopes calculated with the Gogny D1S interaction.

PRC 90, 021301(R) (2014)

Osmium

Prolate deformation $\gamma \approx 0^\circ$ \longrightarrow Transitional nuclei: $\gamma(^{190}\text{Pt}) \approx 30^\circ$, $\gamma(^{192}\text{Pt}) \approx 45^\circ$

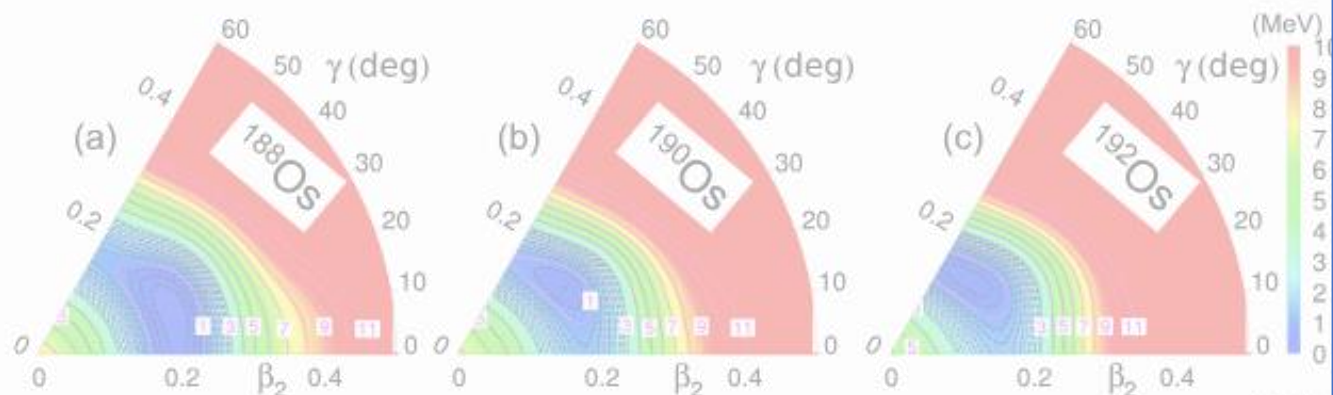


Particle number projected potential energy surfaces in the triaxial plane for $^{188-198}\text{Os}$ isotopes calculated with the Gogny D1S interaction.

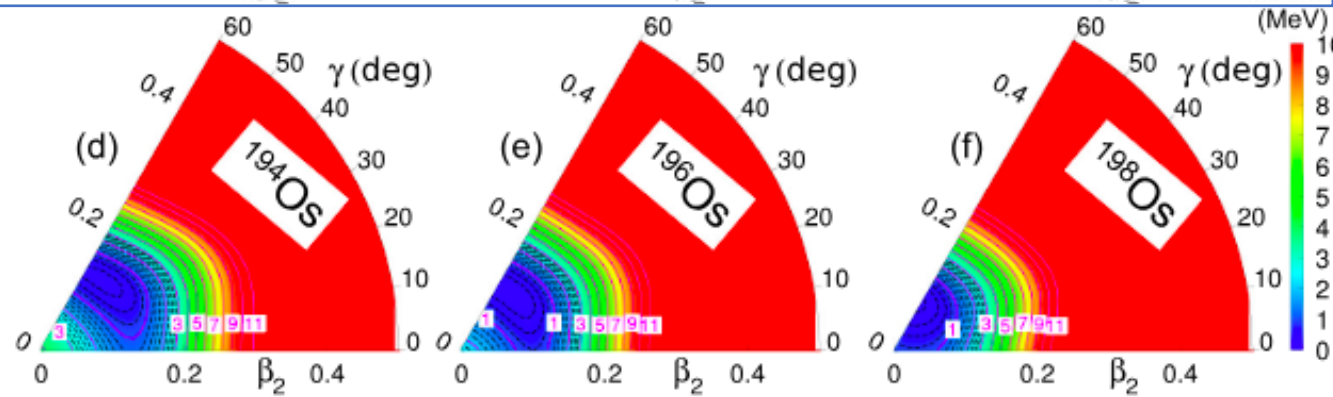
PRC 90, 021301(R) (2014)

Osmium

Prolate deformation $\gamma \approx 0^\circ$ \longrightarrow Transitional nuclei: $\gamma(^{190}\text{Pt}) \approx 30^\circ$, $\gamma(^{192}\text{Pt}) \approx 45^\circ$

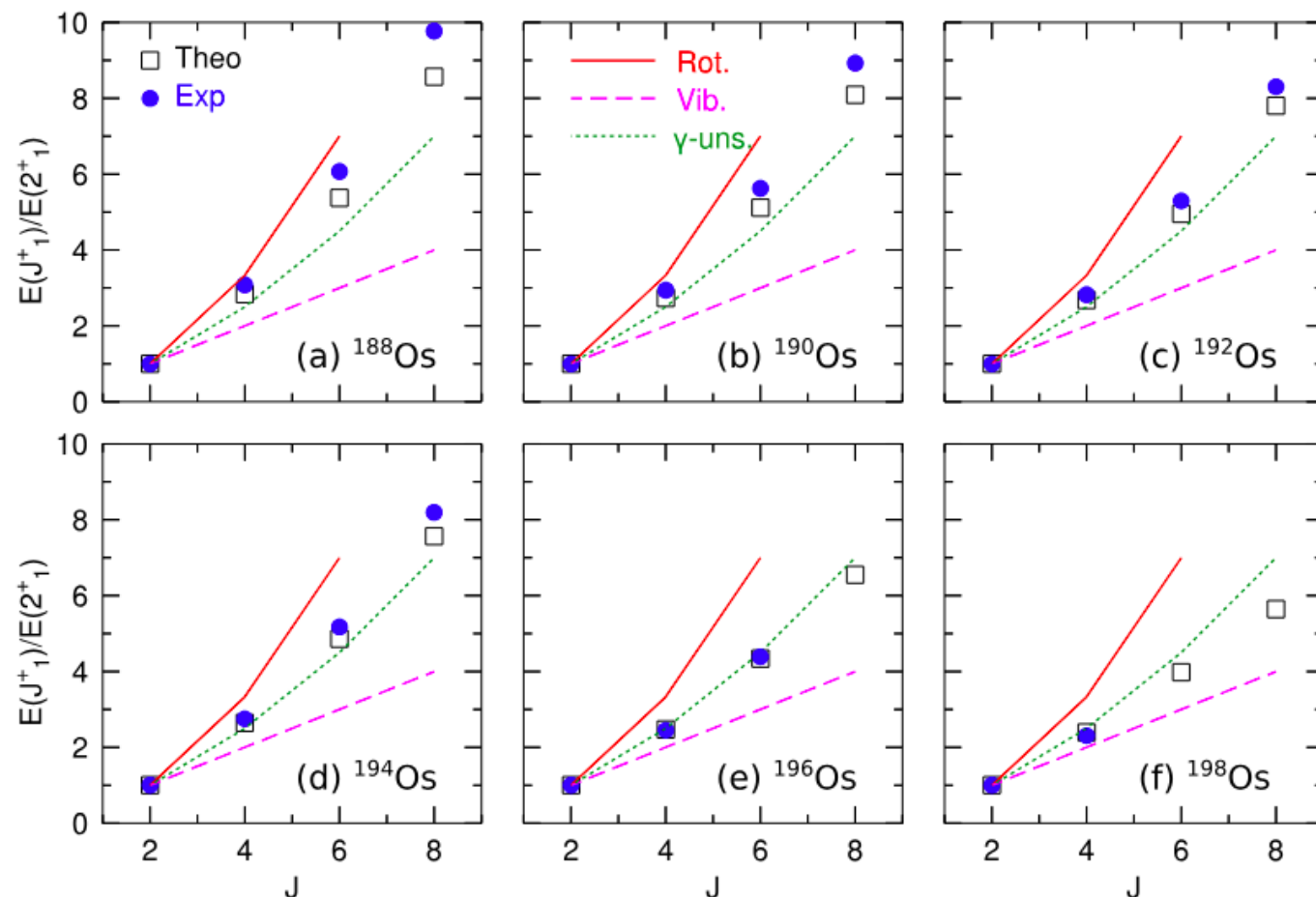


Oblate deformed $\gamma \rightarrow 60^\circ$



Particle number projected potential energy surfaces in the triaxial plane for $^{188-198}\text{Os}$ isotopes calculated with the Gogny D1S interaction.

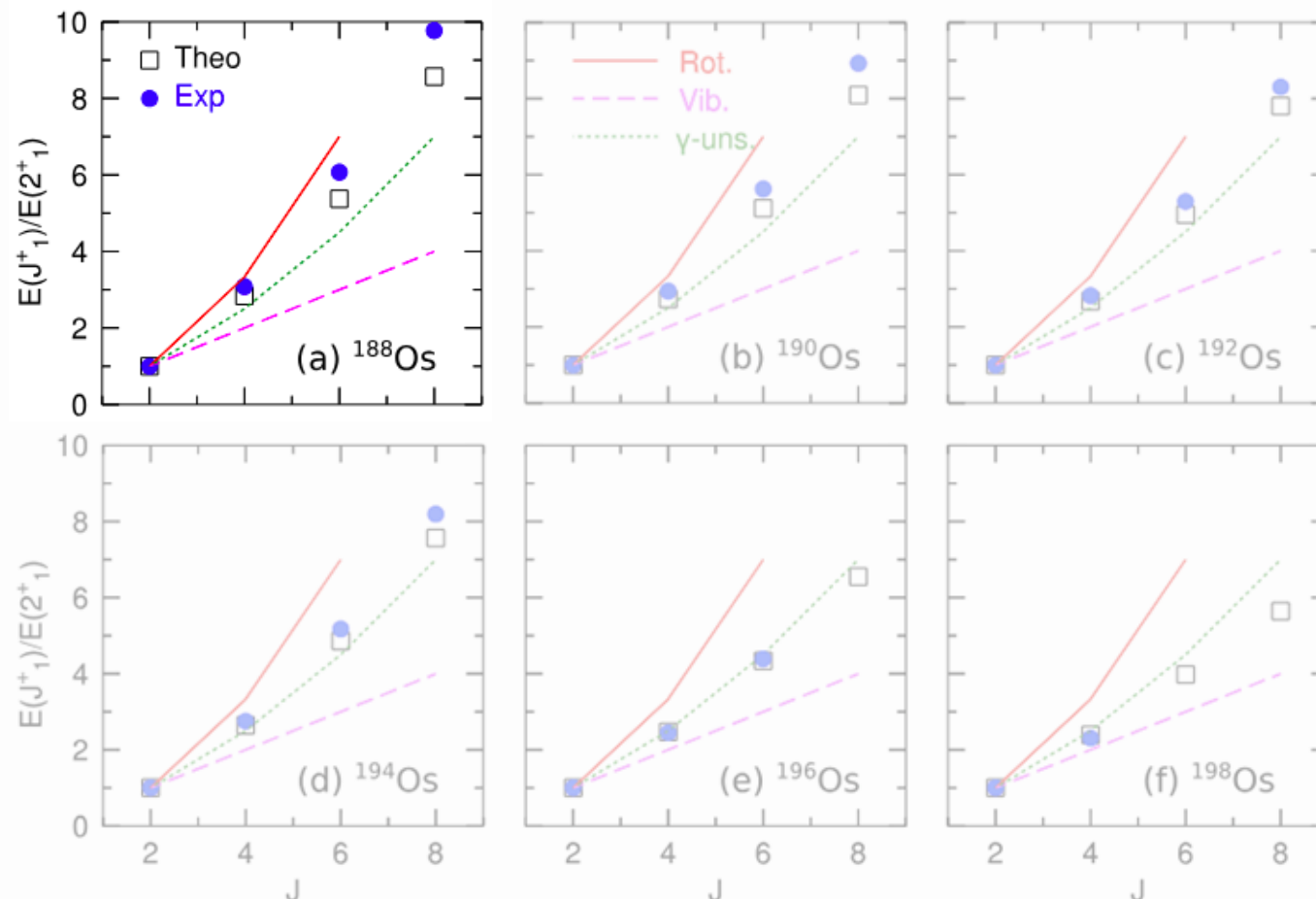
Osmium



Yrast band excitation energies, normalized to the corresponding 2_1^+ energies, for $^{188-198}\text{Os}$ isotopes. Blue dots and black boxes are the experimental points and theoretical beyond-mean-field predictions, respectively.

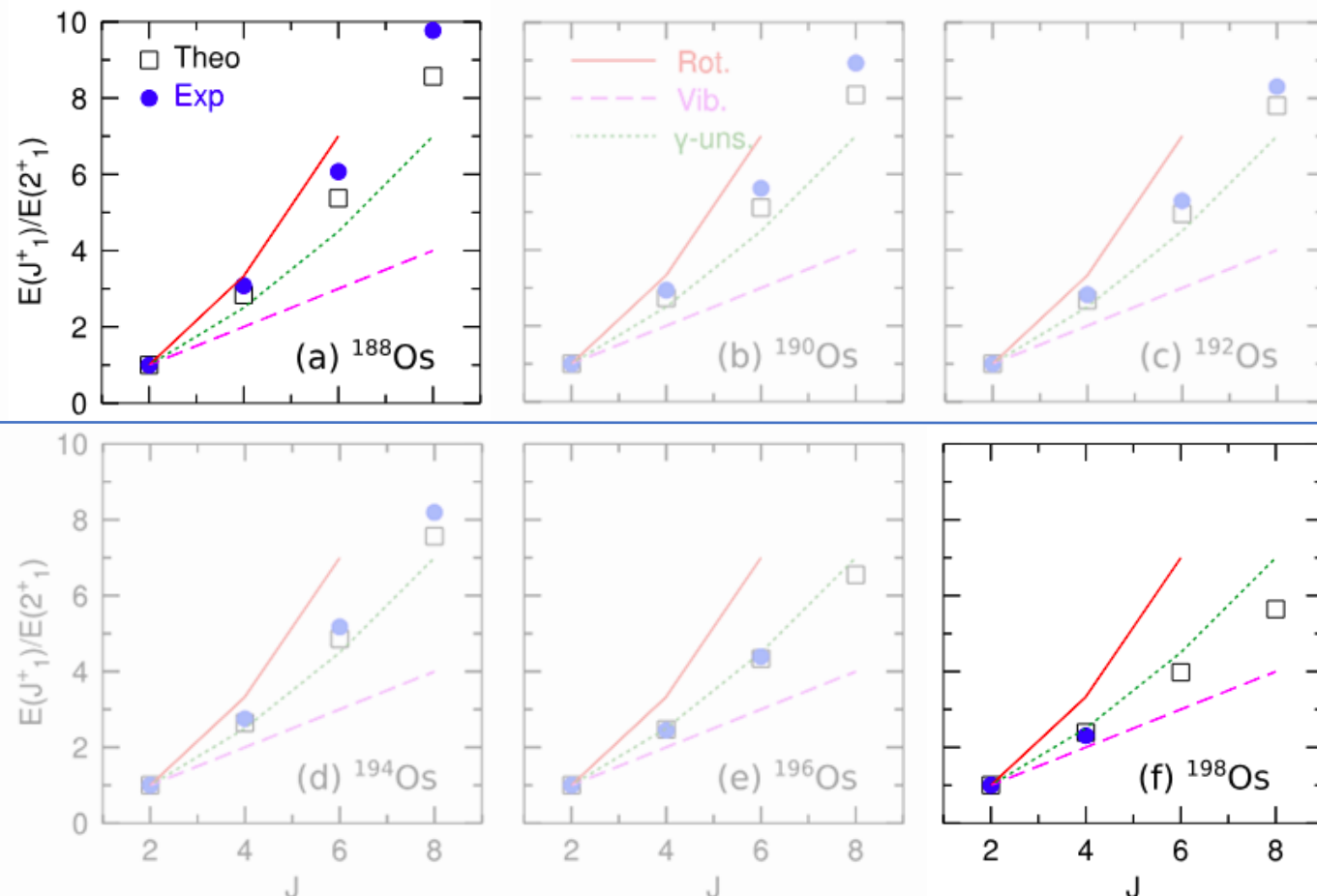
Osmium

Axial rotational



Yrast band excitation energies, normalized to the corresponding 2^+_{1} energies, for $^{188-198}\text{Os}$ isotopes. Blue dots and black boxes are the experimental points and theoretical beyond-mean-field predictions, respectively.

Osmium

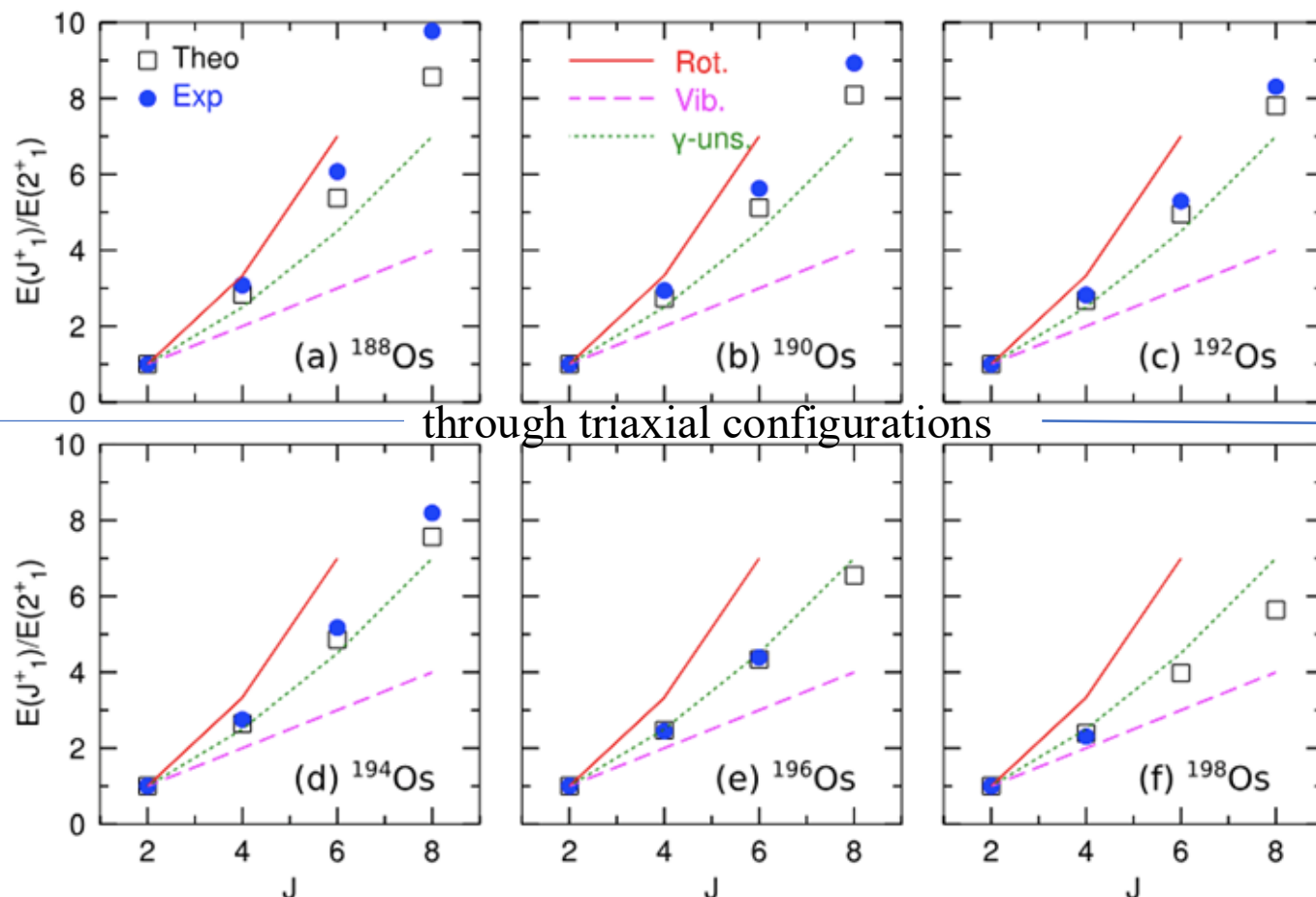


Axial rotational

More vibrational

Yrast band excitation energies, normalized to the corresponding 2_1^+ energies, for $^{188-198}\text{Os}$ isotopes. Blue dots and black boxes are the experimental points and theoretical beyond-mean-field predictions, respectively.

Osmium



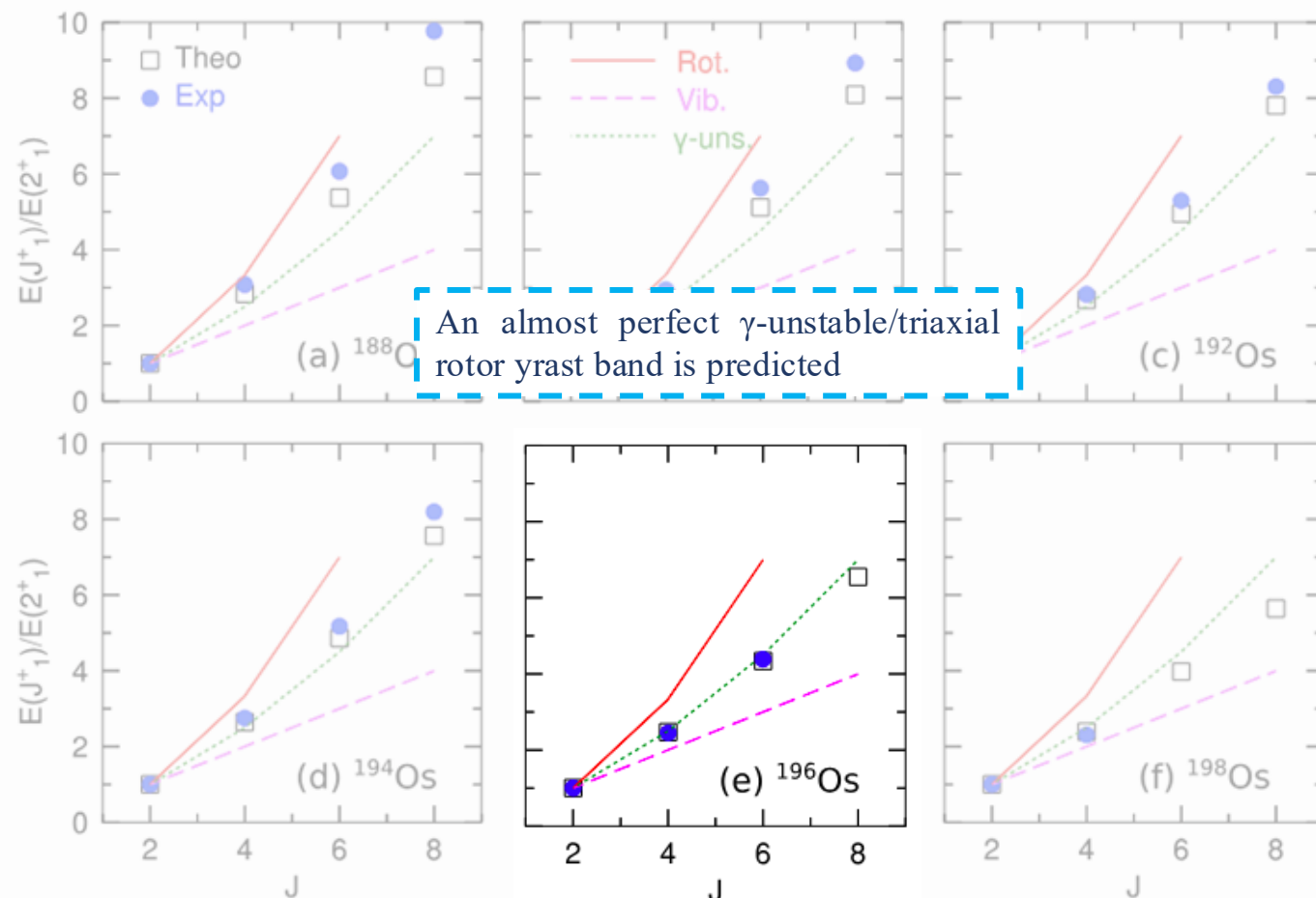
Axial rotational

through triaxial configurations

More vibrational

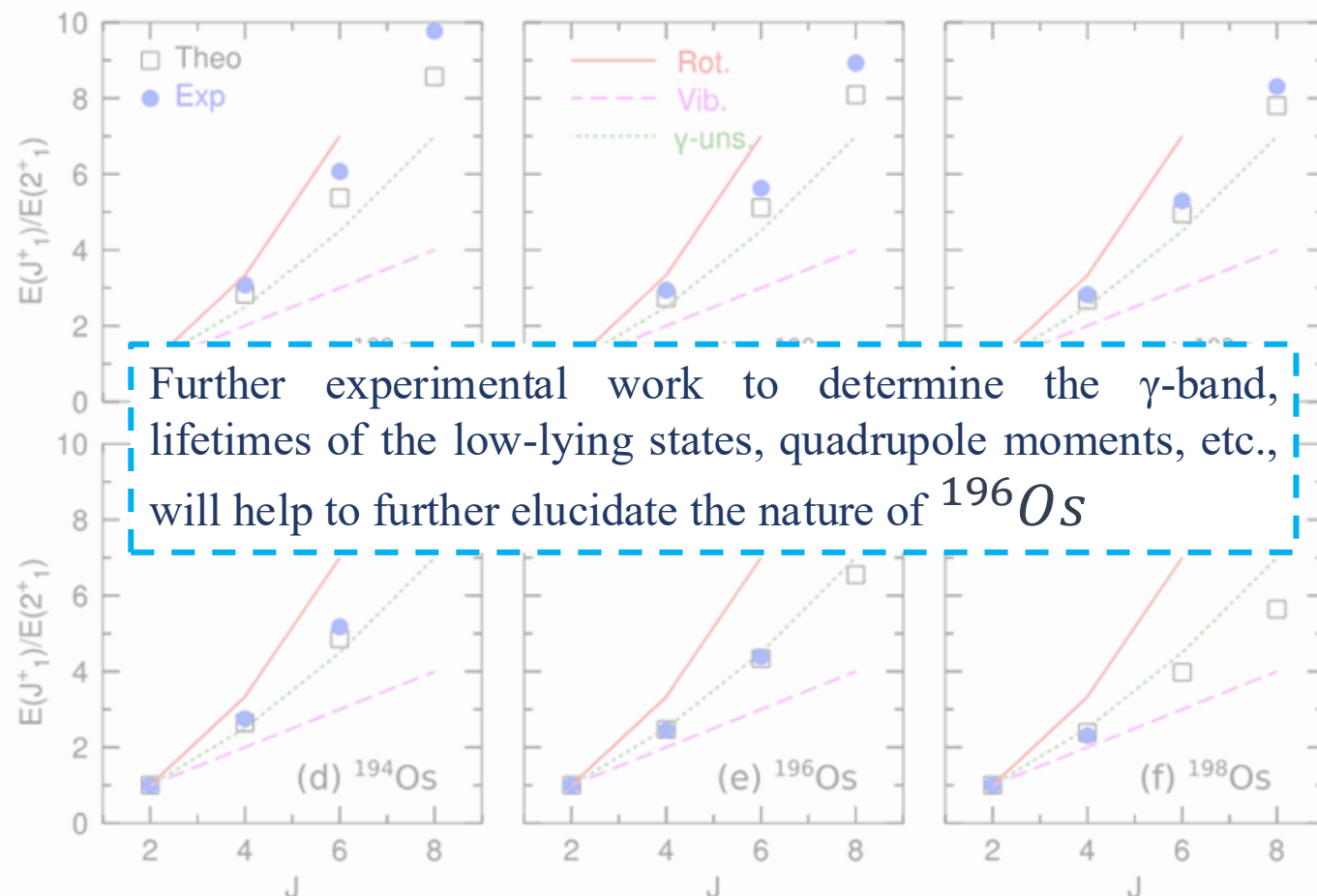
Yrast band excitation energies, normalized to the corresponding 2_1^+ energies, for $^{188-198}\text{Os}$ isotopes. Blue dots and black boxes are the experimental points and theoretical beyond-mean-field predictions, respectively.

Osmium



Yrast band excitation energies, normalized to the corresponding 2_1^+ energies, for $^{188-198}\text{Os}$ isotopes. Blue dots and black boxes are the experimental points and theoretical beyond-mean-field predictions, respectively.

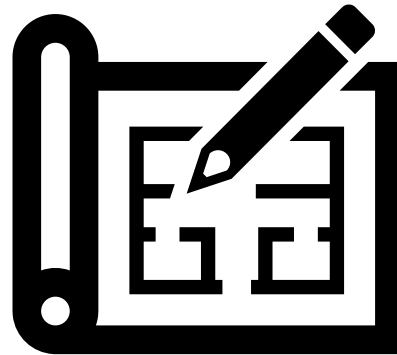
Osmium



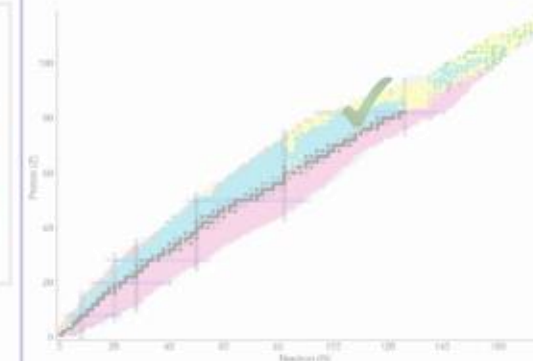
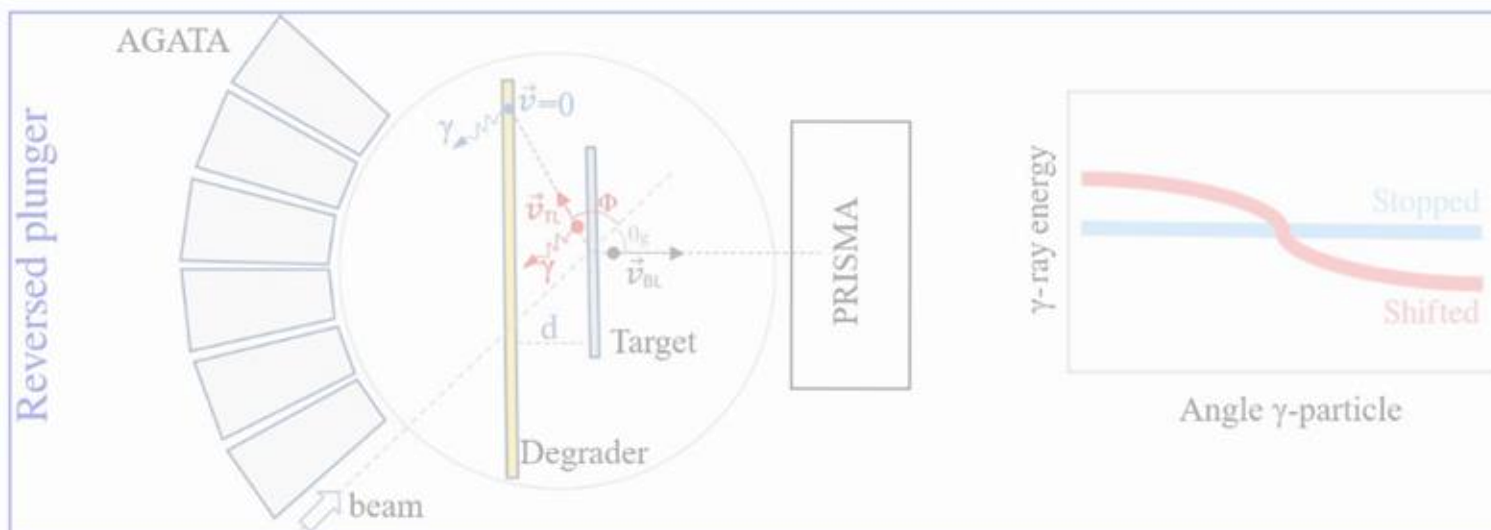
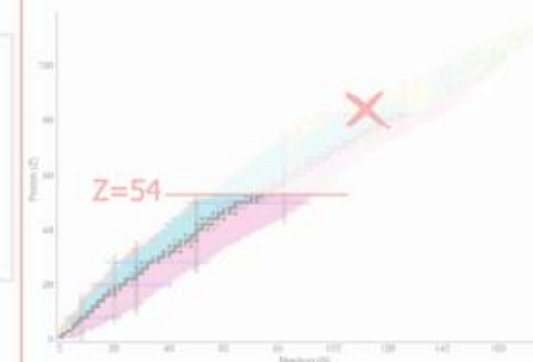
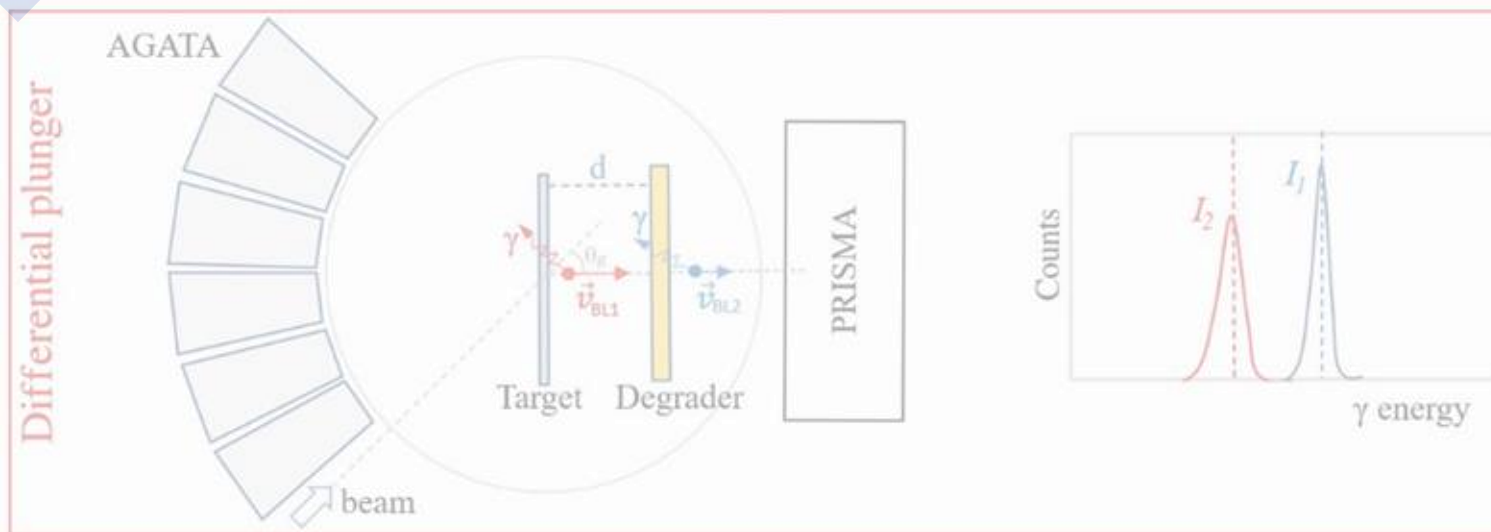
Yrast band excitation energies, normalized to the corresponding 2_1^+ energies, for $^{188-198}\text{Os}$ isotopes. Blue dots and black boxes are the experimental points and theoretical beyond-mean-field predictions, respectively.



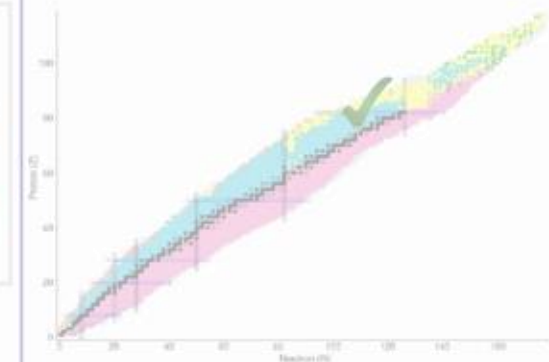
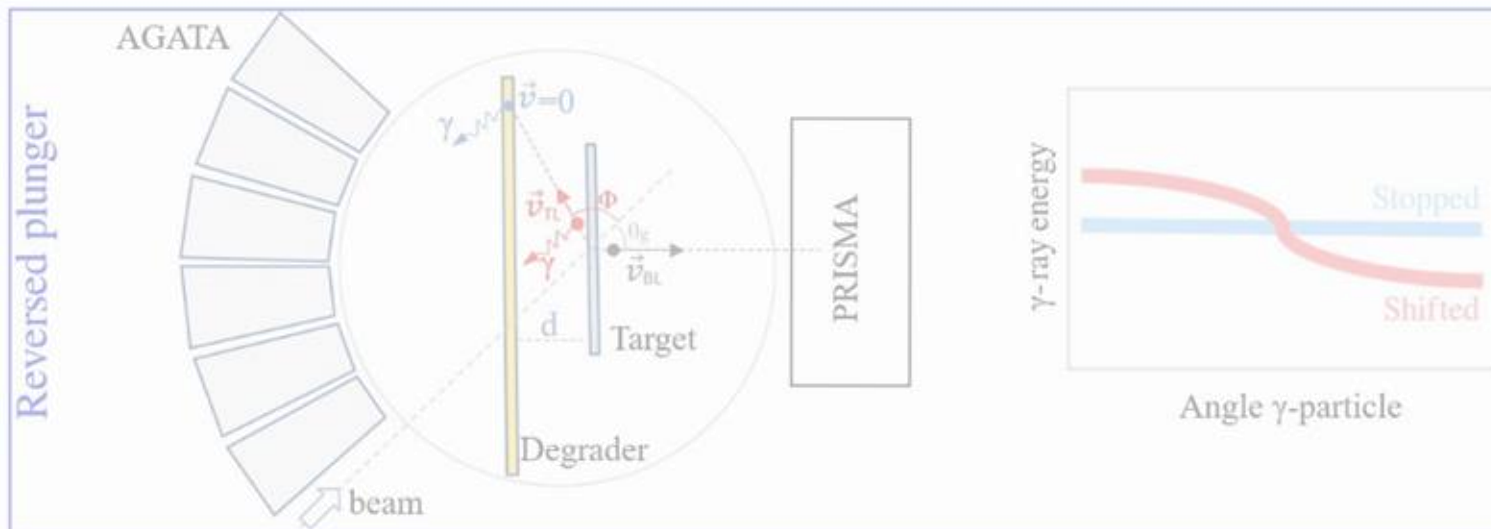
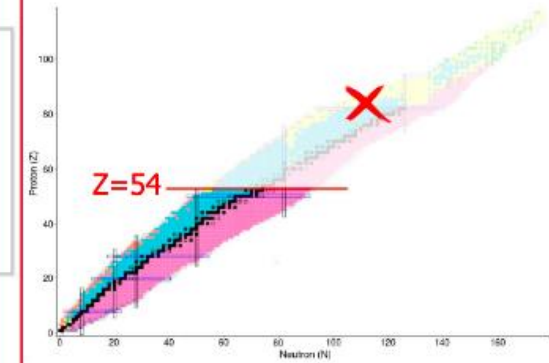
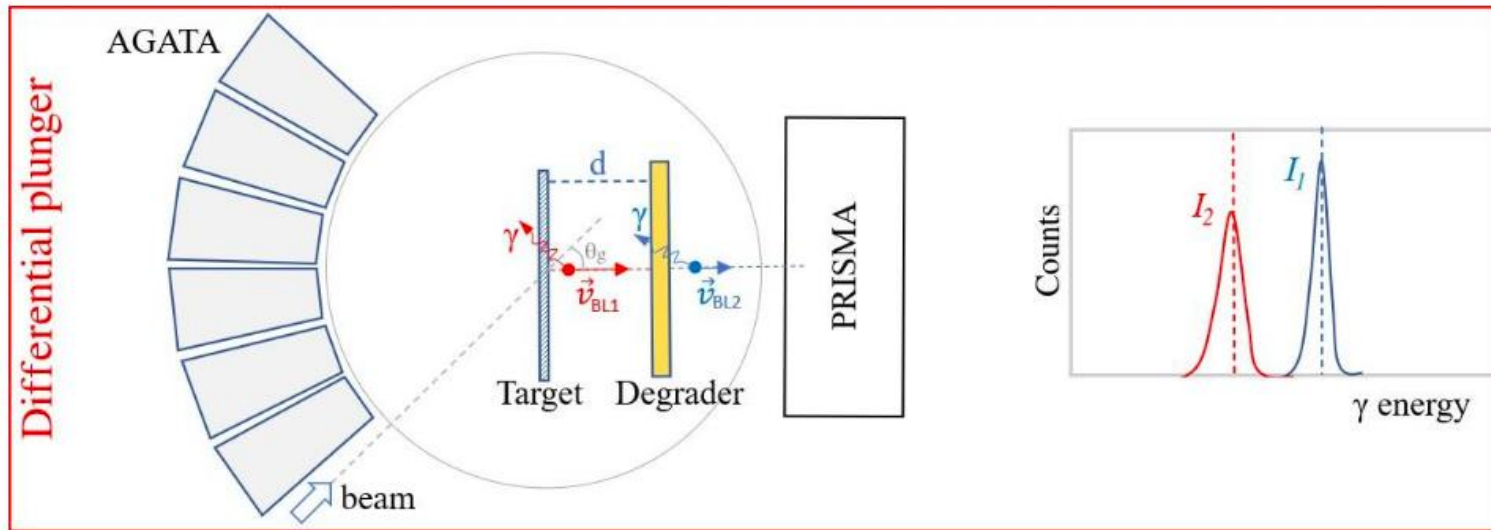
Reversed Plunger



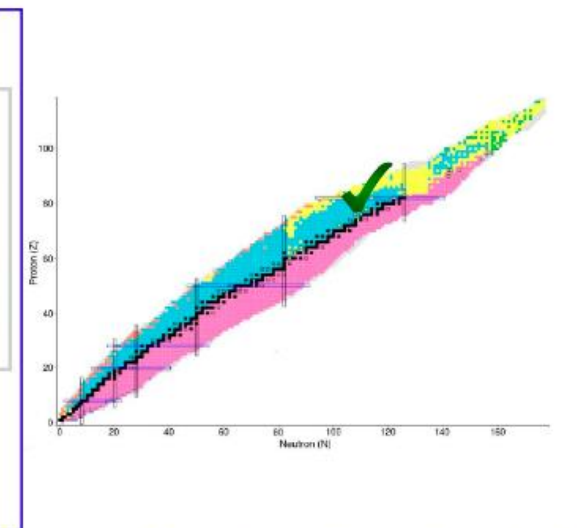
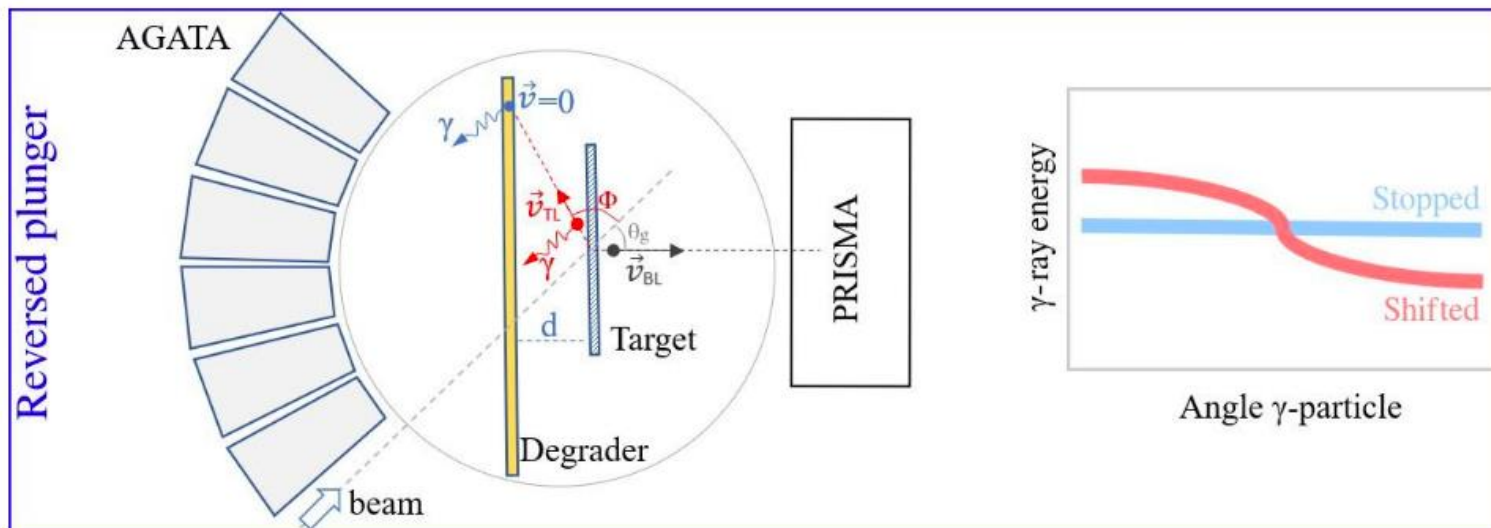
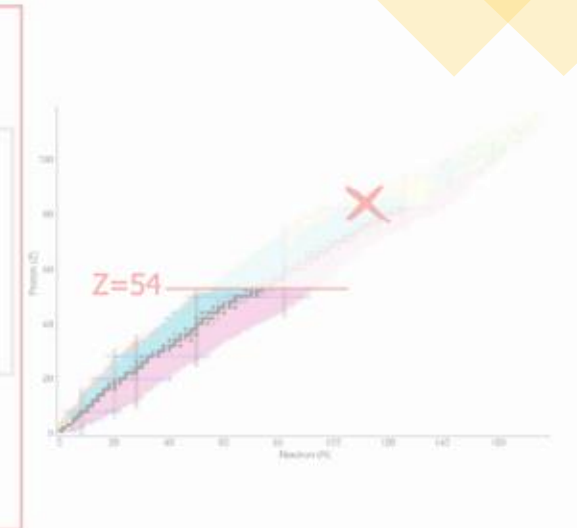
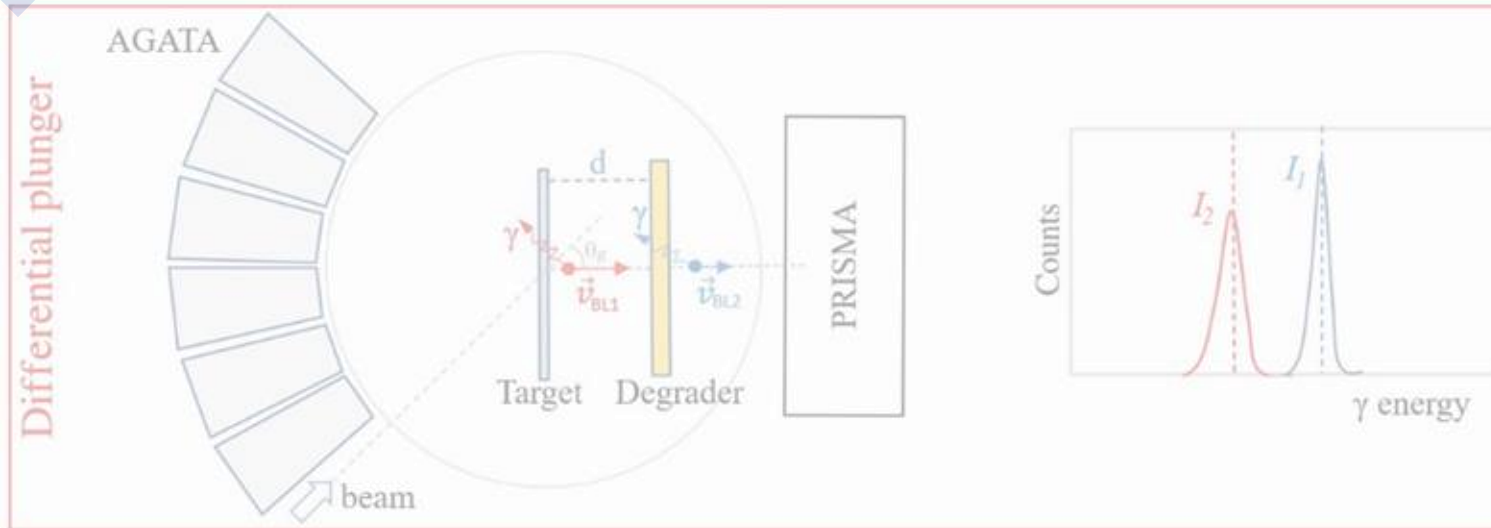
The Reversed Plunger Technique for Lifetime Measurements



The Reversed Plunger Technique for Lifetime Measurements



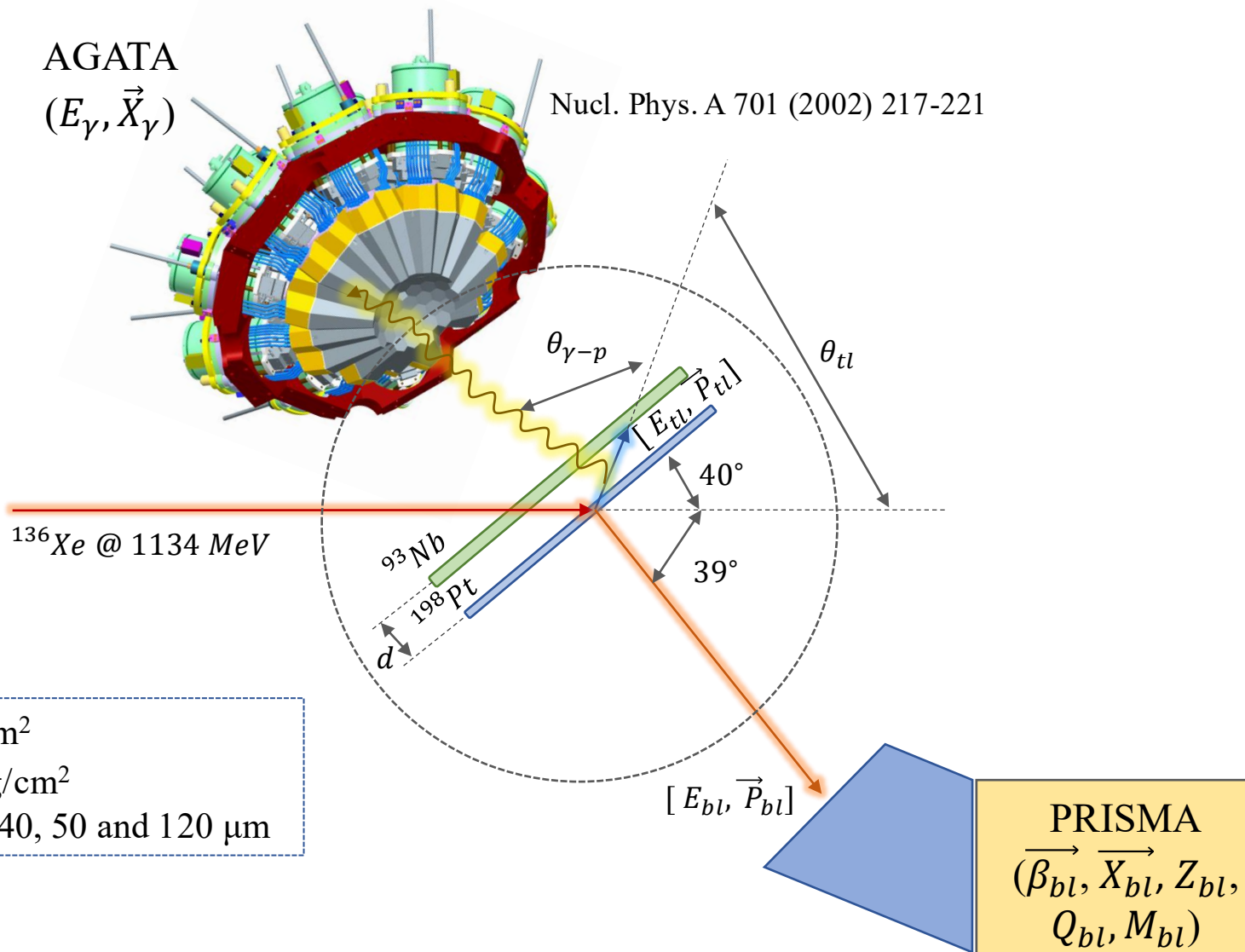
The Reversed Plunger Technique for Lifetime Measurements



Experimental Details

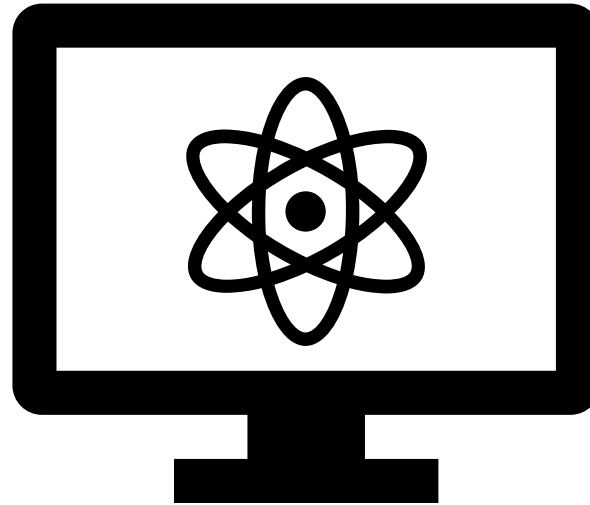
AGATA
(E_γ, \vec{X}_γ)

Nucl. Phys. A 701 (2002) 217-221



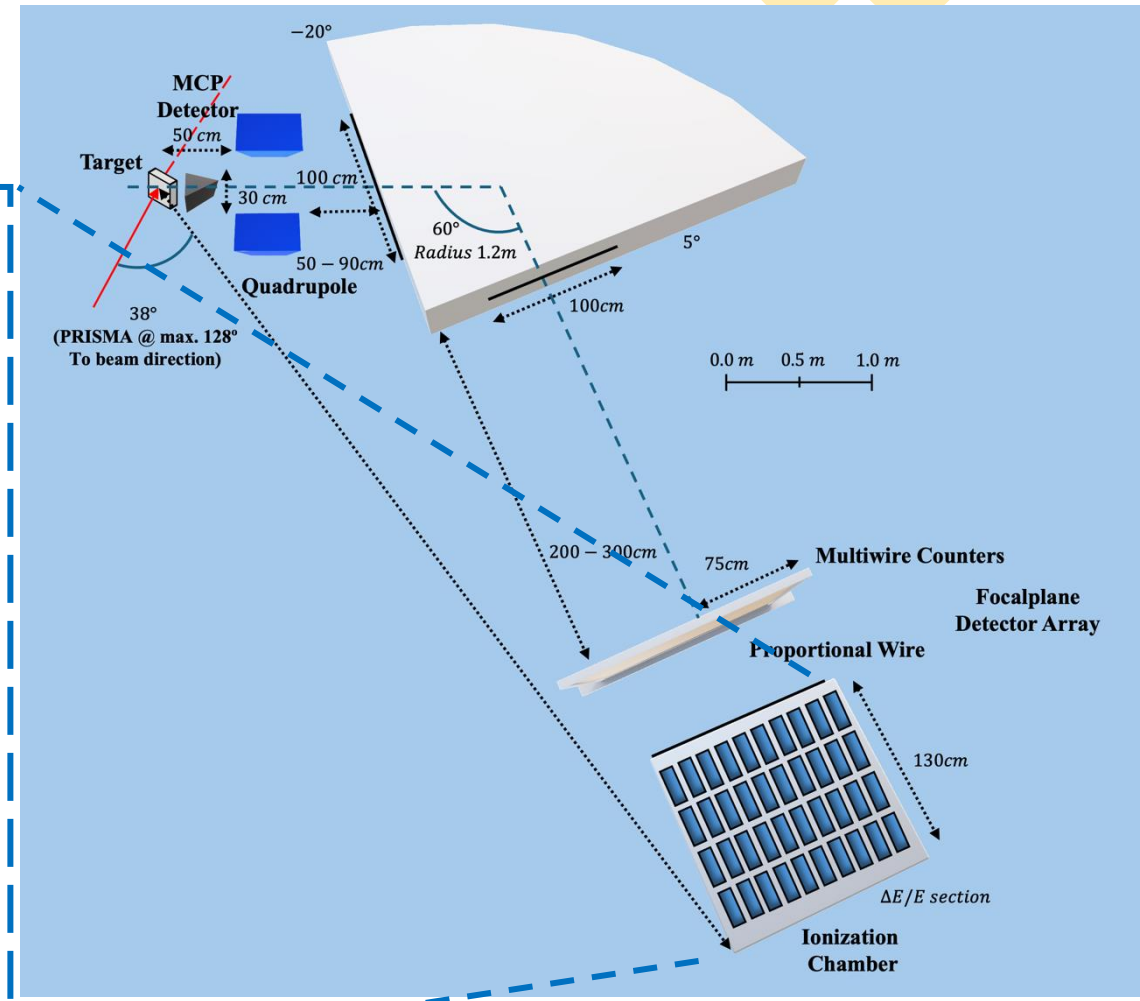
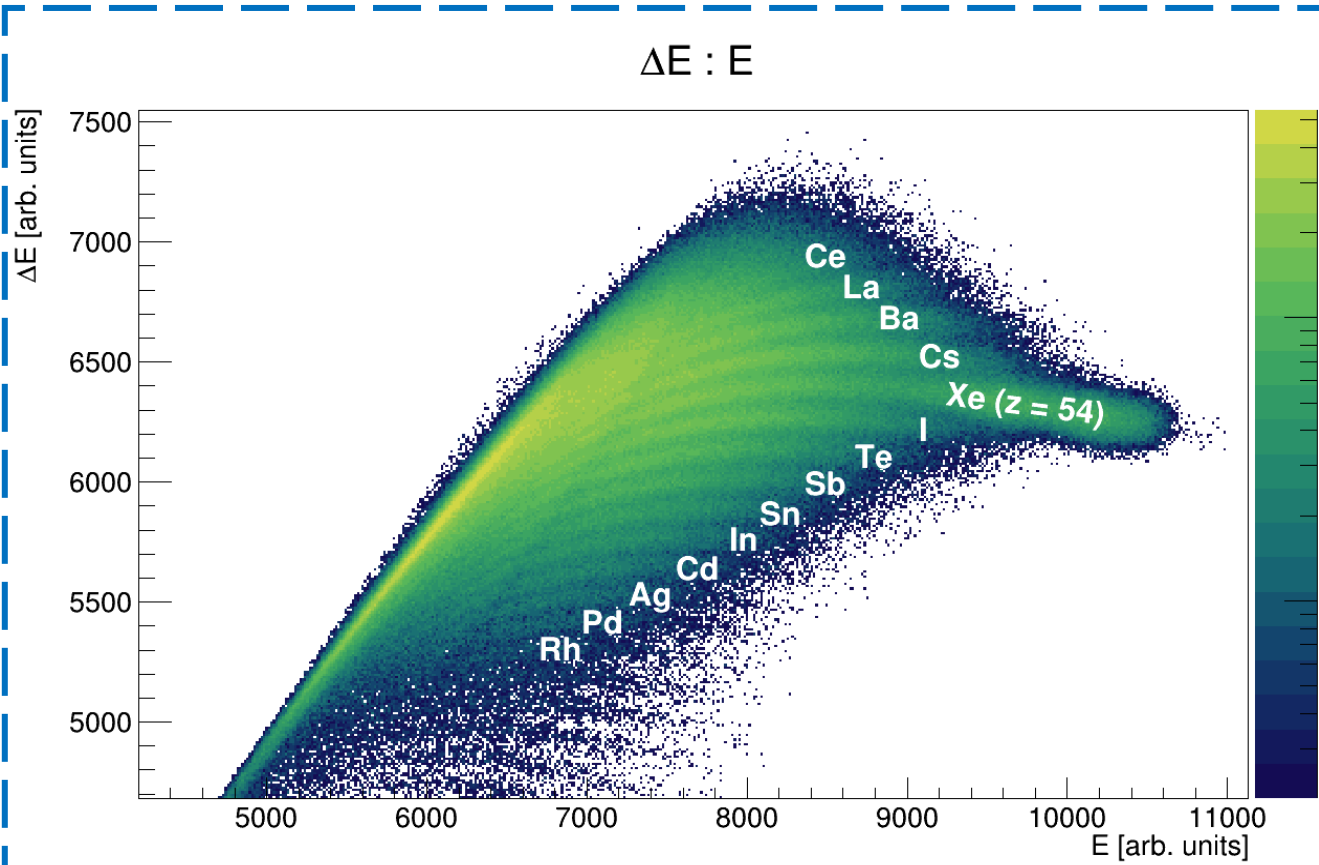
^{198}Pt target: 1.4 mg/cm²
 ^{93}Nb degrader: 3.2 mg/cm²
 Plunger distances: 30, 40, 50 and 120 μm

Nucl. Phys. A 701 (2002) 217-221



Analysis

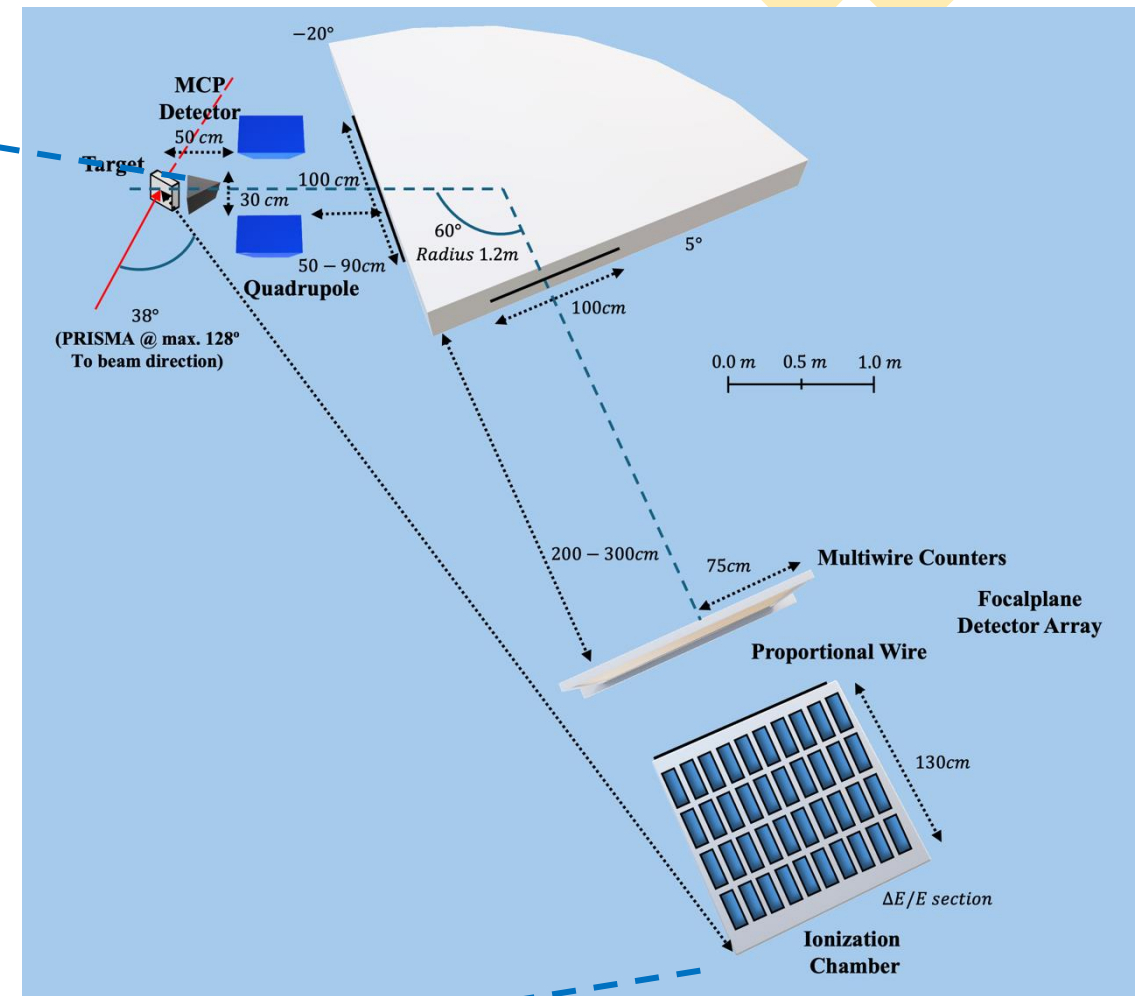
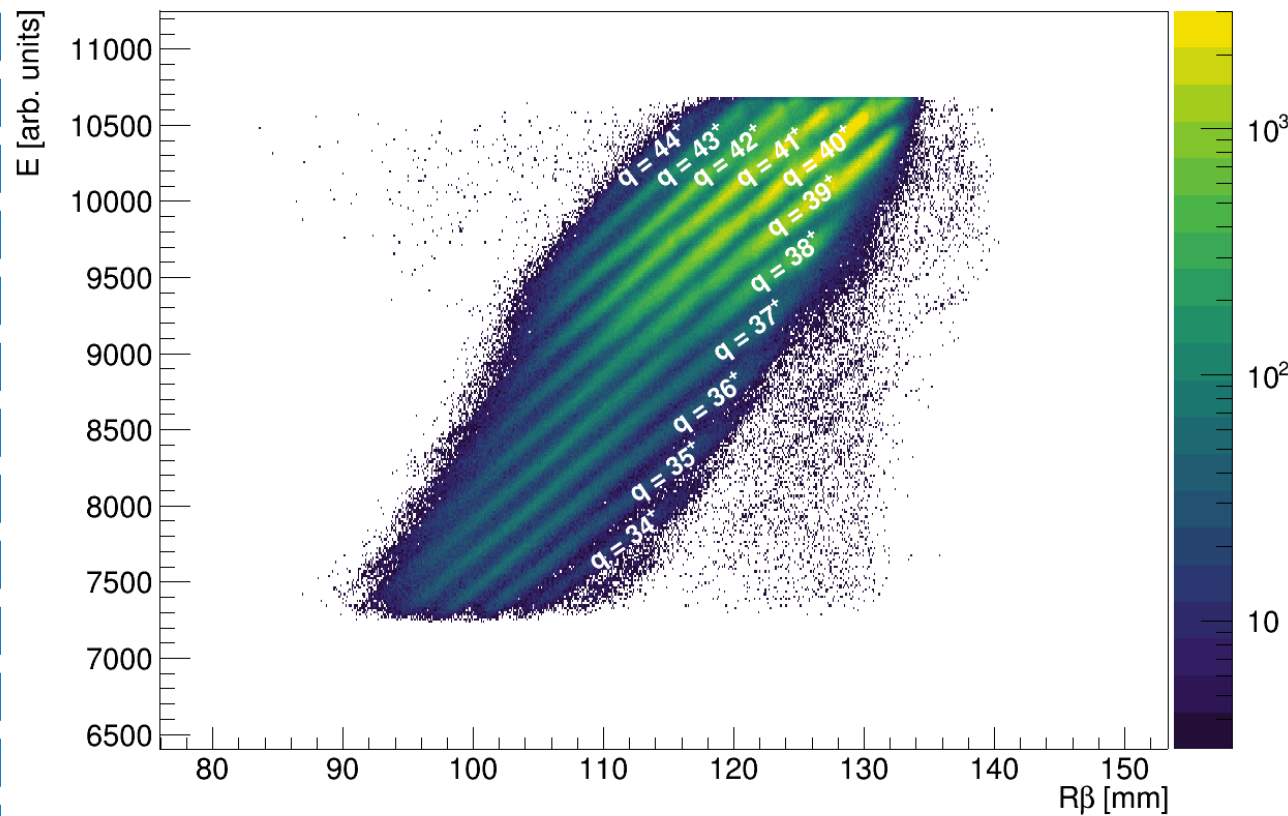
Z Identification



Nuc. Instr. and Meth. A 1049 (2023) 168040

Charge States

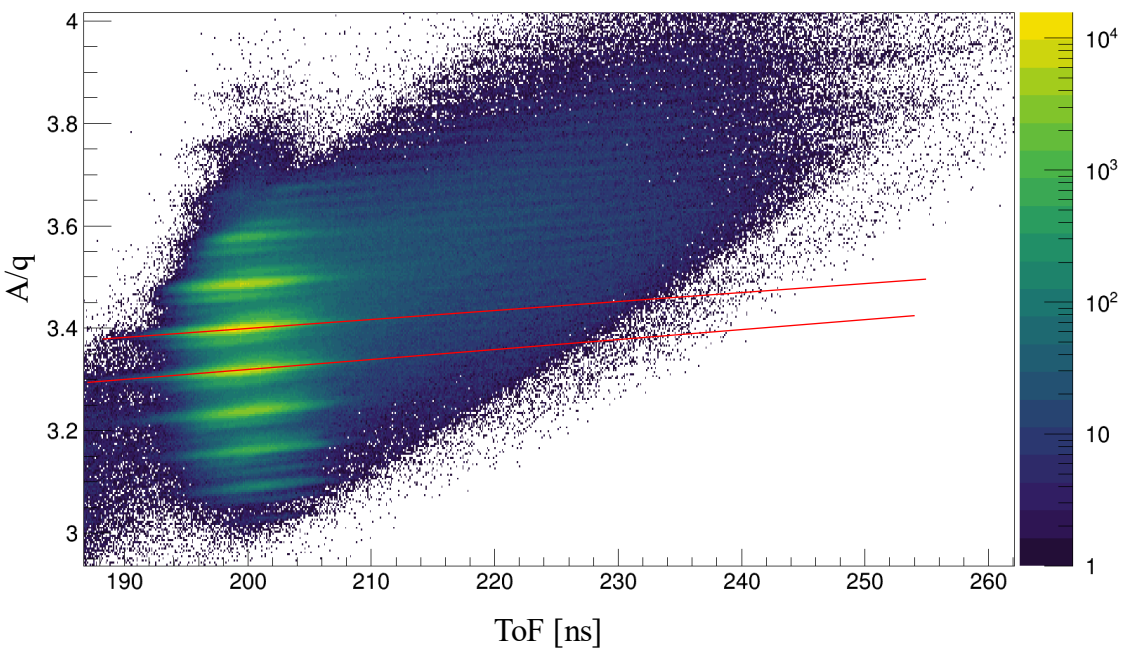
$E_{IC} : R\beta (Z = 54)$



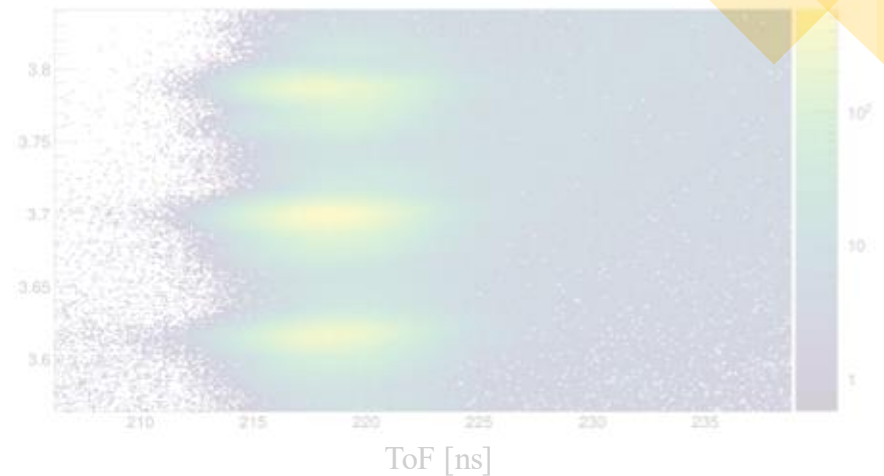
Nuc. Instr. and Meth. A 1049 (2023) 168040

A/q Analysis

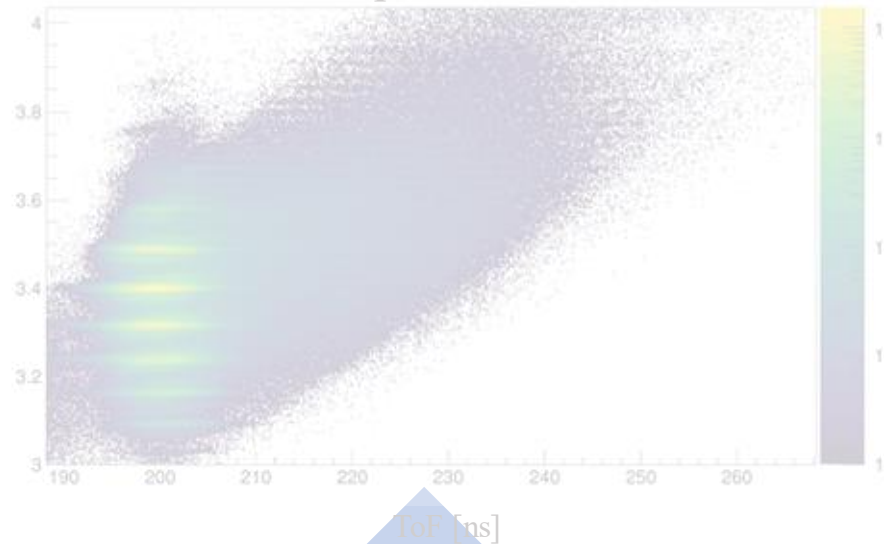
A/q : TOF (Z = 54)



$ToF + 22 ns$

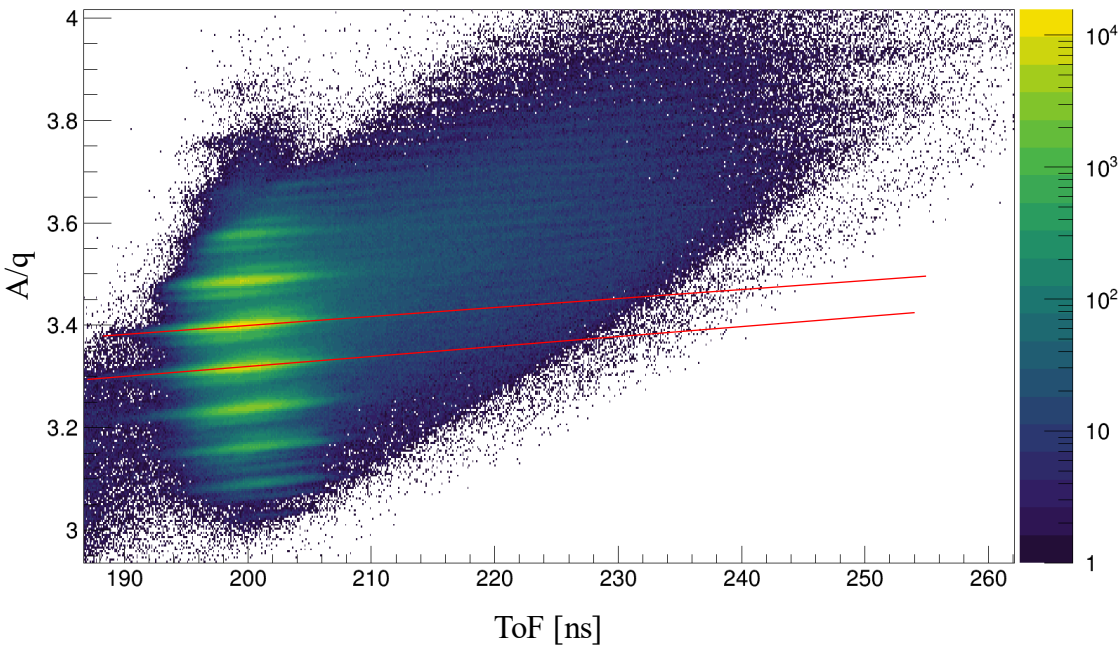


Slope Correction

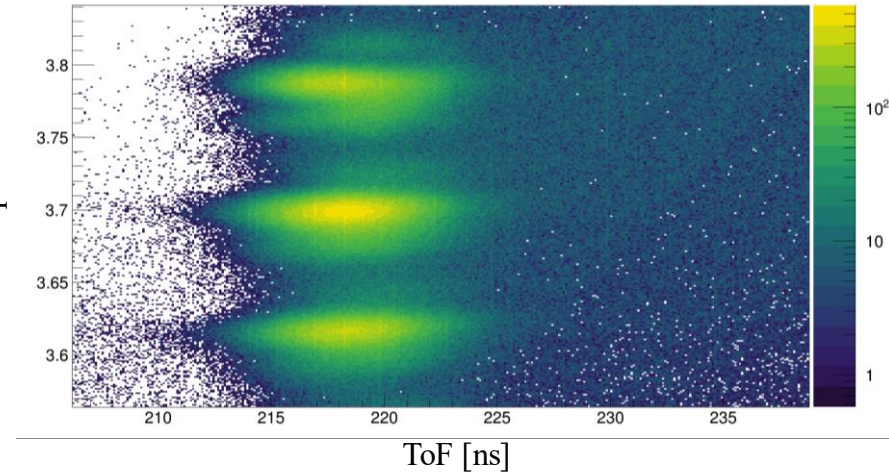


A/q Analysis

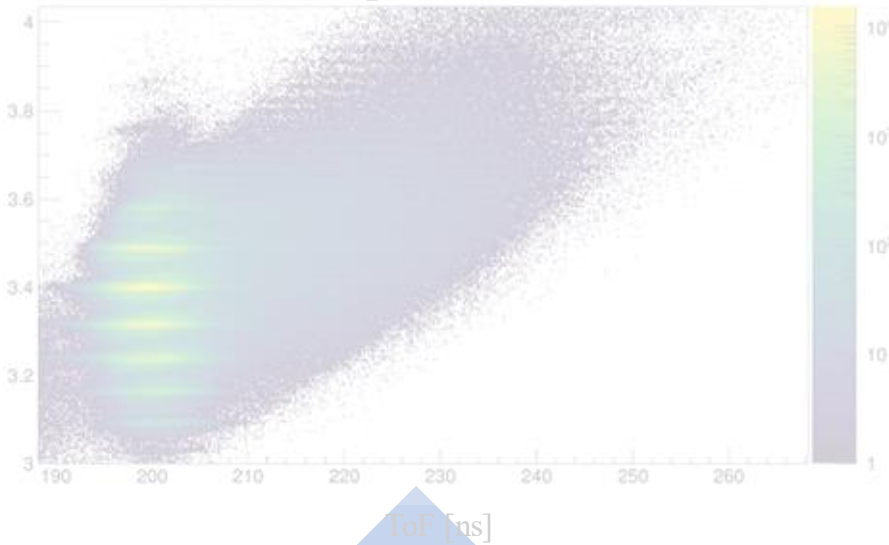
A/q : TOF (Z = 54)



ToF + 22 ns

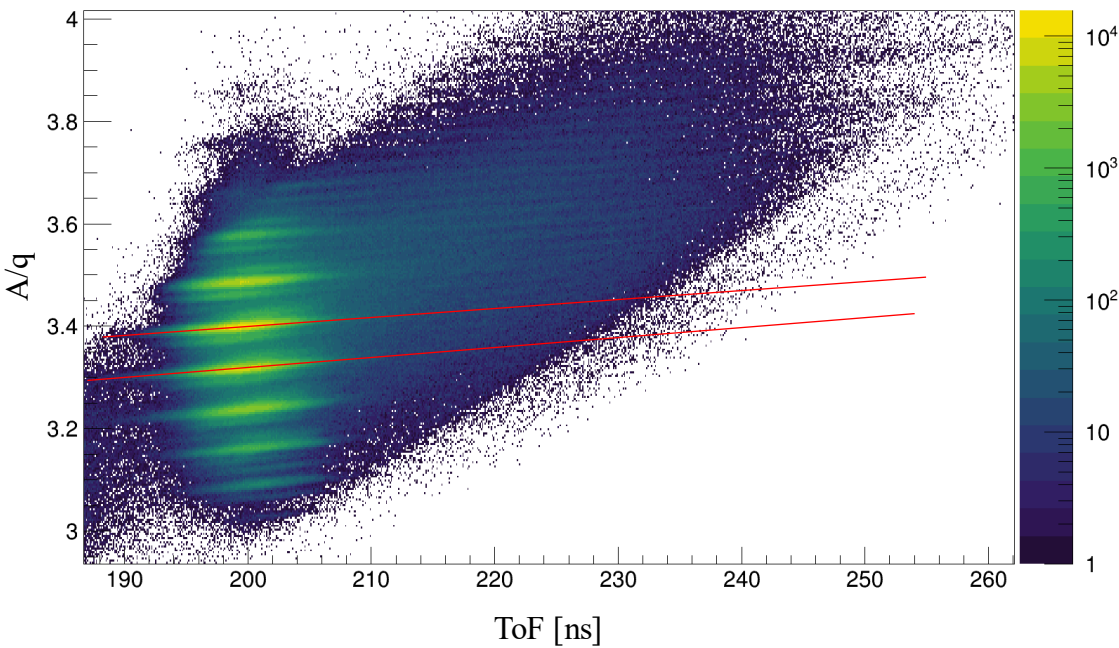


Slope Correction

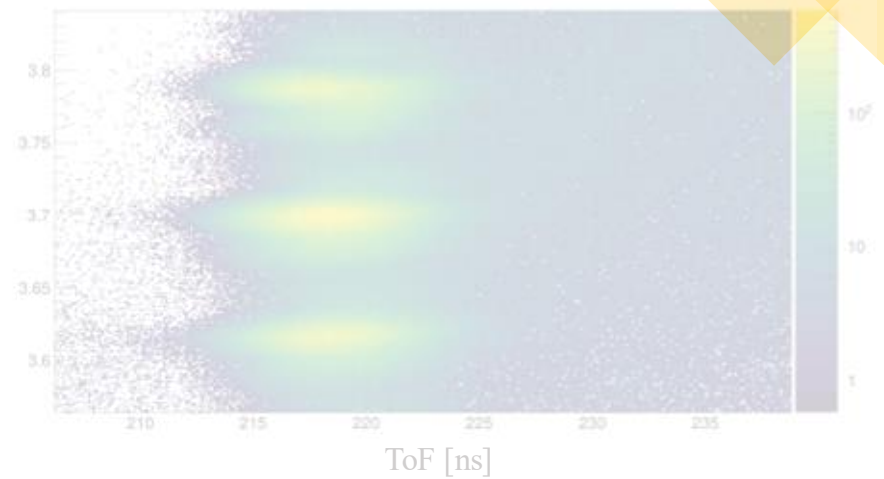


A/q Analysis

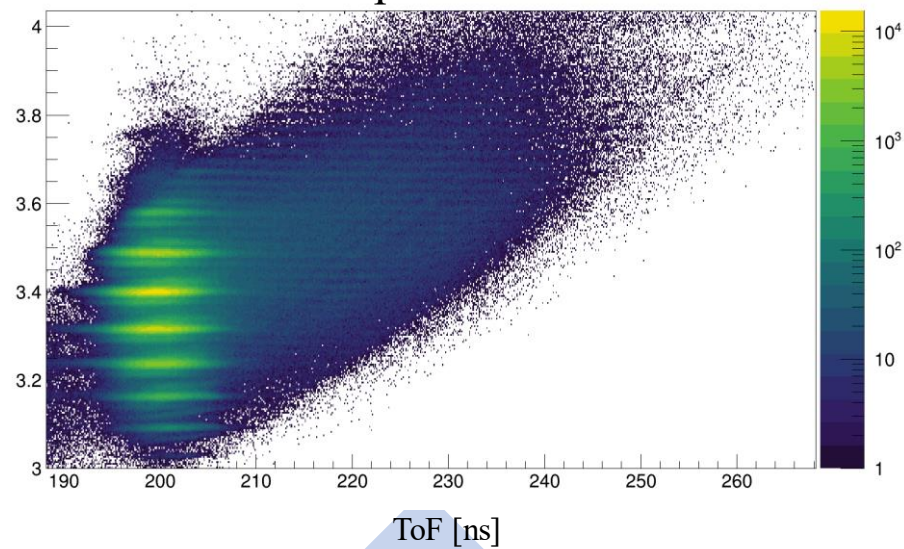
A/q : TOF (Z = 54)



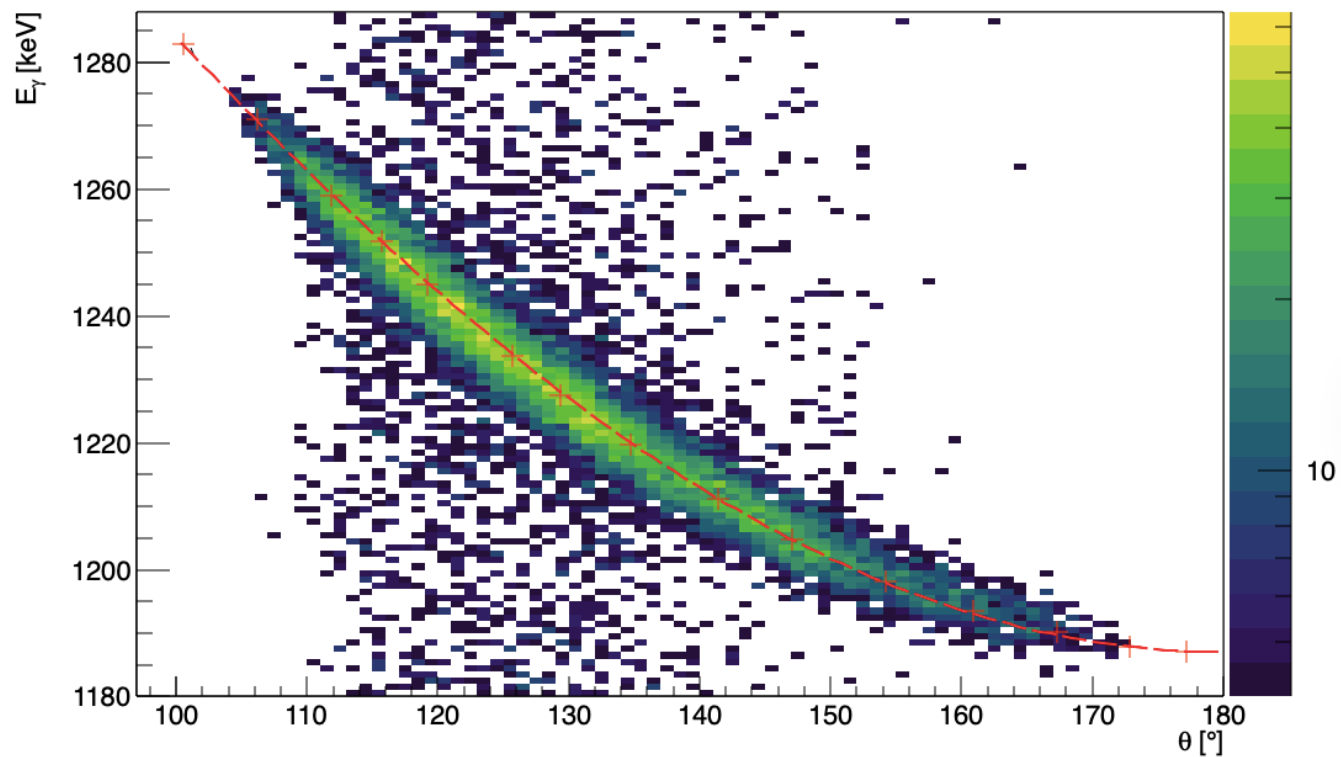
ToF + 22 ns



Slope Correction



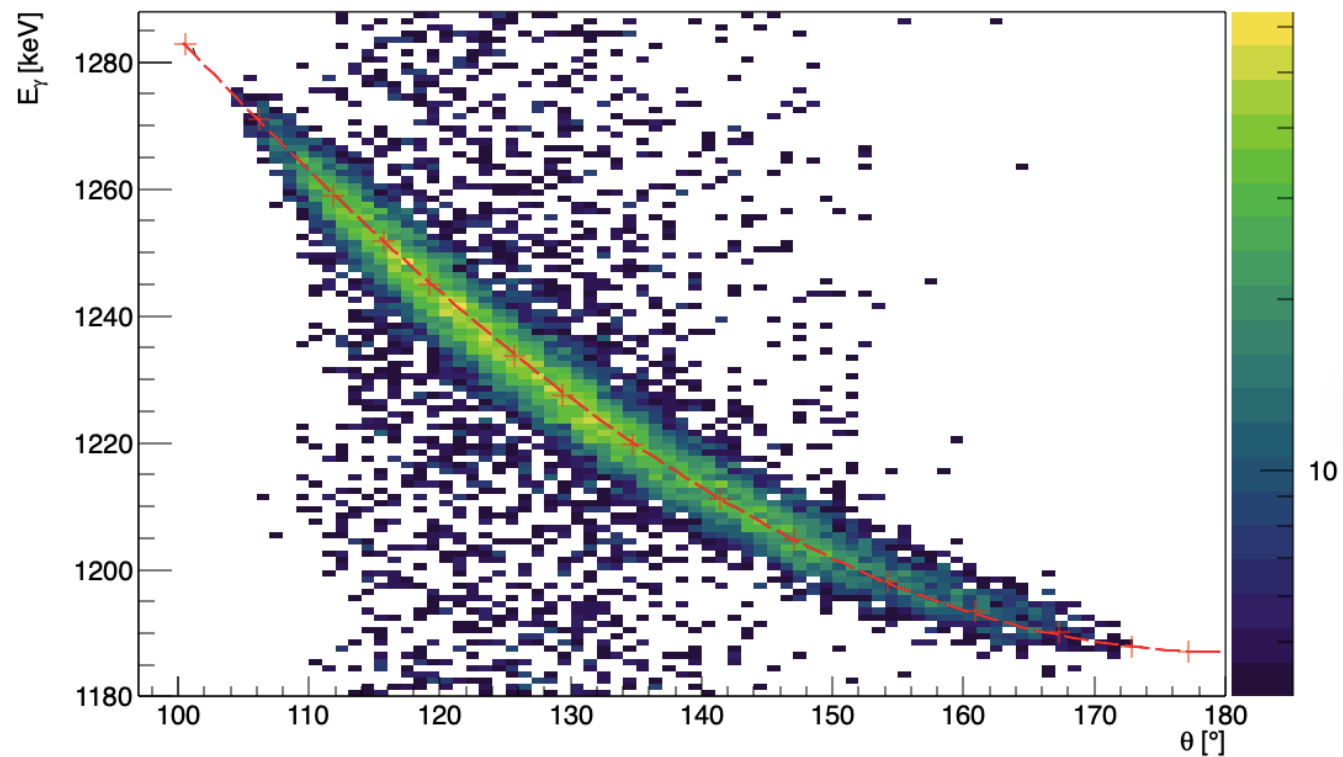
$\beta_{136}\chi_e$ Estimation



$$E'_\gamma = E_\gamma \frac{\sqrt{1 - \beta^2}}{1 - \beta \cos \theta}$$

$$\beta \approx 0.101$$

$\beta_{136}\chi_e$ Estimation



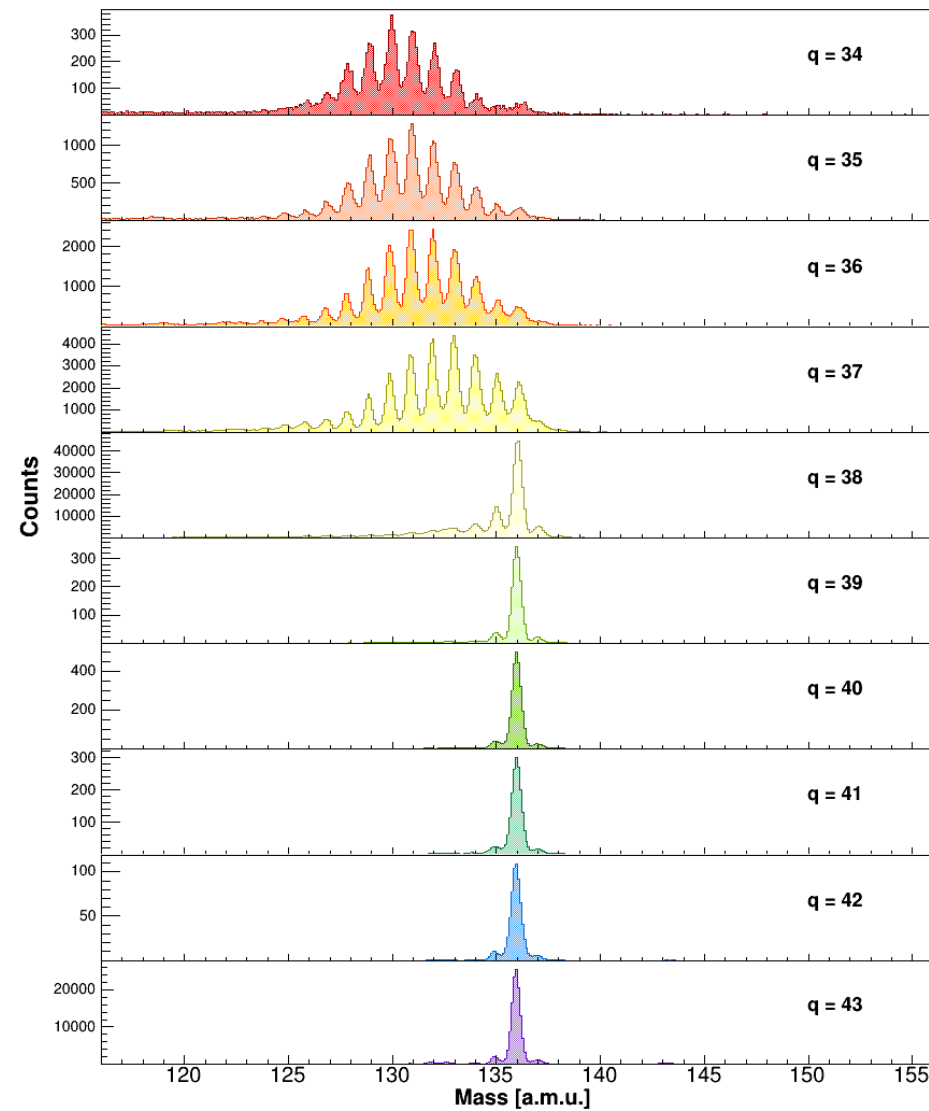
$$E'_\gamma = E_\gamma \frac{\sqrt{1 - \beta^2}}{1 - \beta \cos \theta}$$

NO +22ns OFFSET is needed!

$$\beta \approx 0.101$$

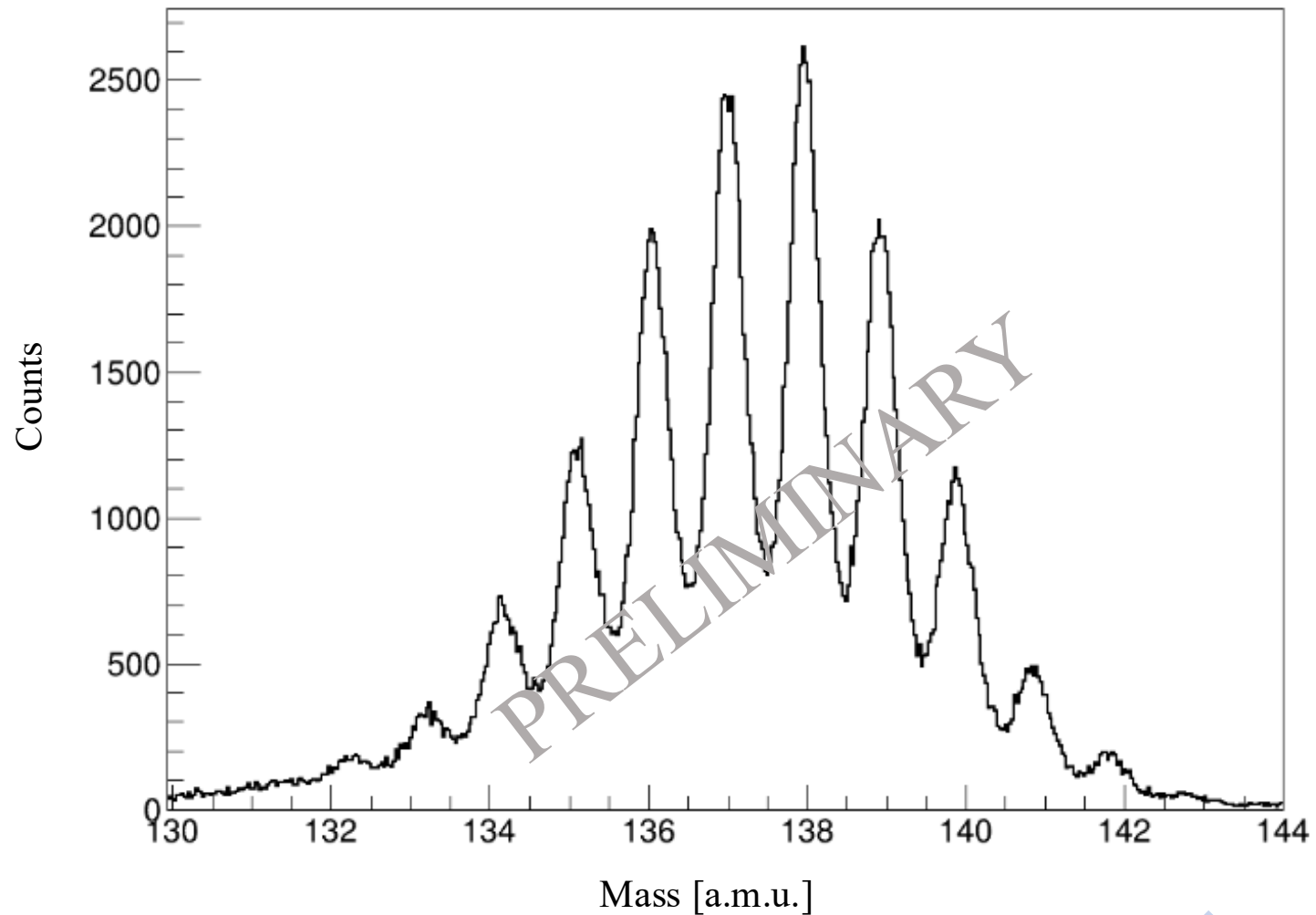


Mass Distribution ($Z = 54$)

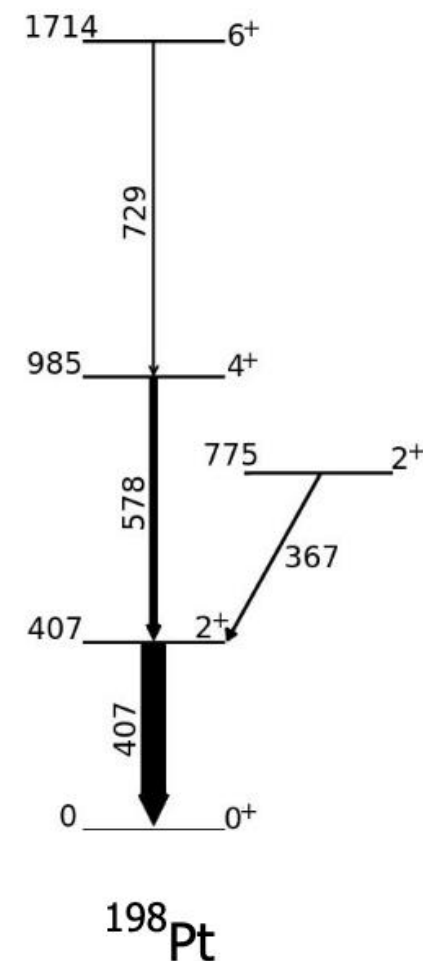
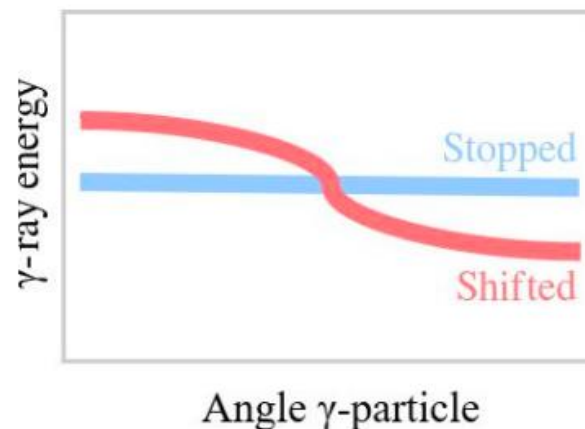
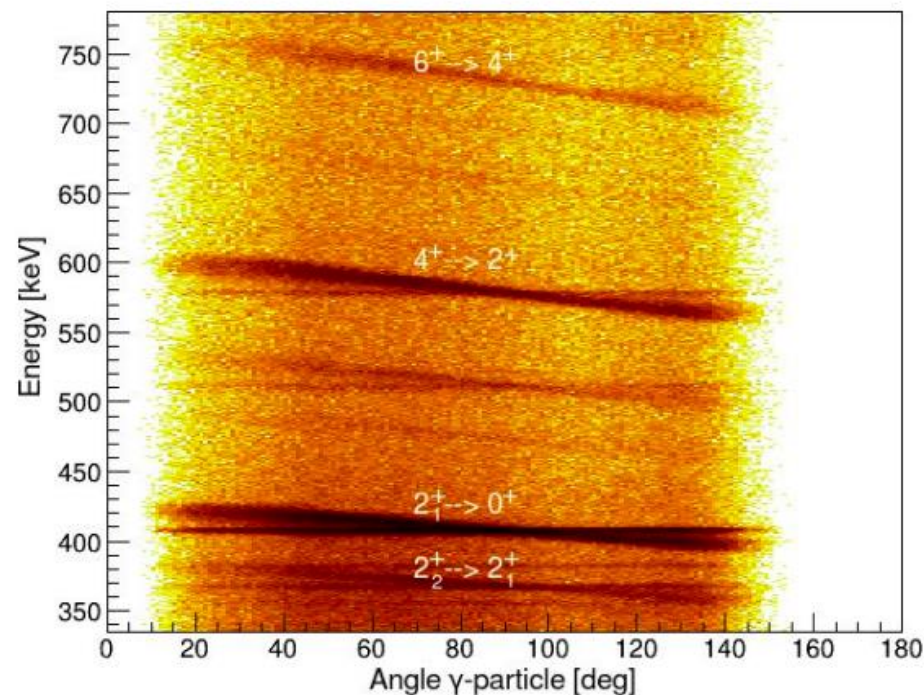




Mass Distribution ($Z = 56$)

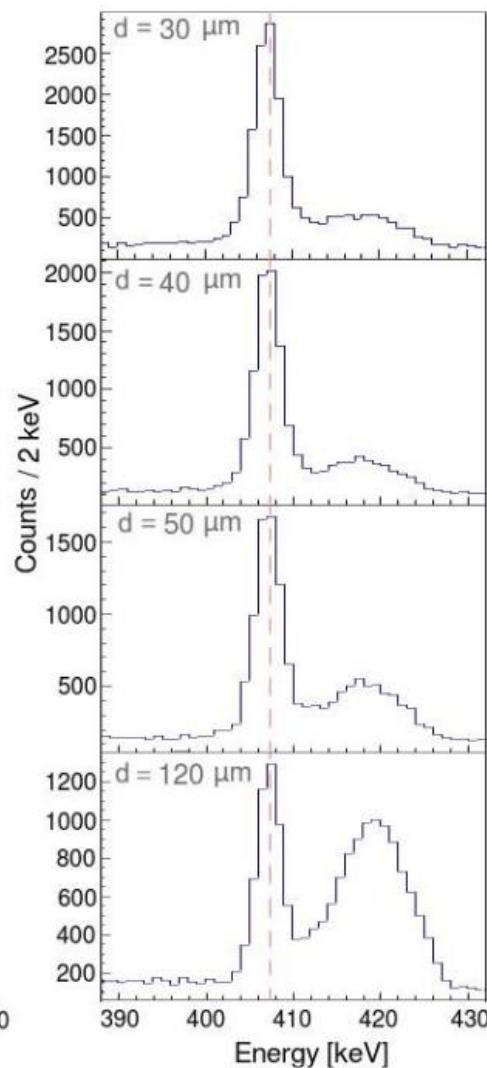
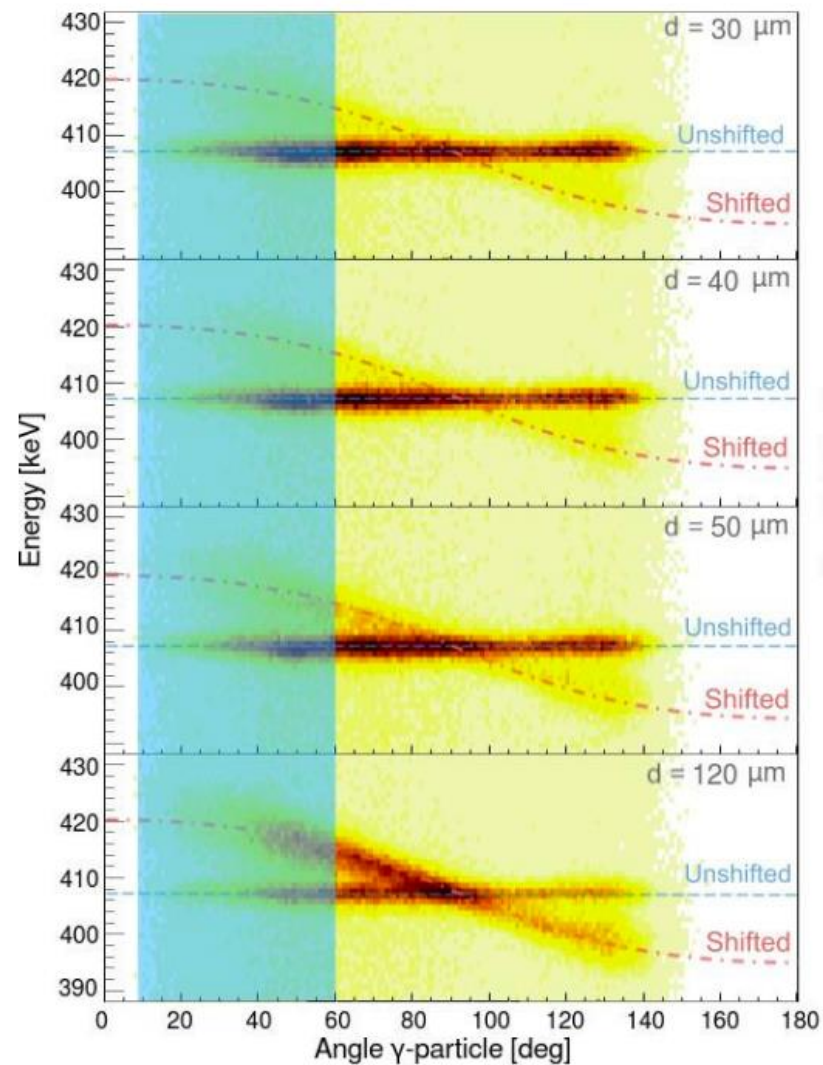


The Line Shape Matrix for ^{198}Pt

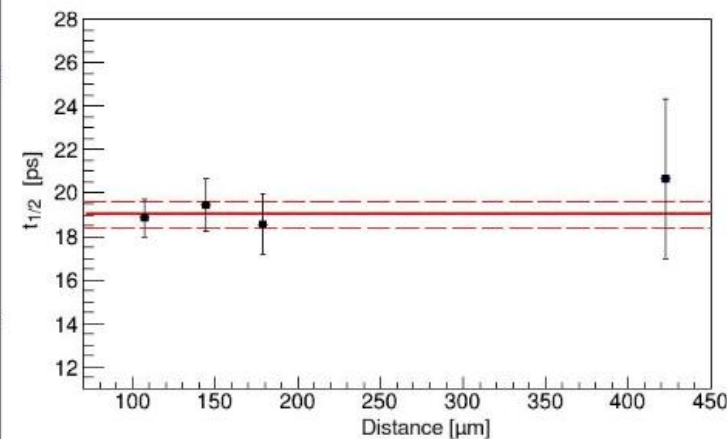


- The 407-keV transition ($2_1^+ \rightarrow 0^+$) (shifted+stopped component)
- The 578-keV transition ($4^+ \rightarrow 2_1^+$) (shifted+stopped component)
- The 367-keV transition ($2_2^+ \rightarrow 2_1^+$) (shifted+stopped component)
- The 729-keV transition ($6^+ \rightarrow 4^+$) (shifted component)

Lifetime Measurement of the 2_1^+



$$\tau_i = \frac{-R_i(t) + \sum b_{ki} \alpha_{ki} R_k(t)}{\frac{dR_i(t)}{dt}}$$

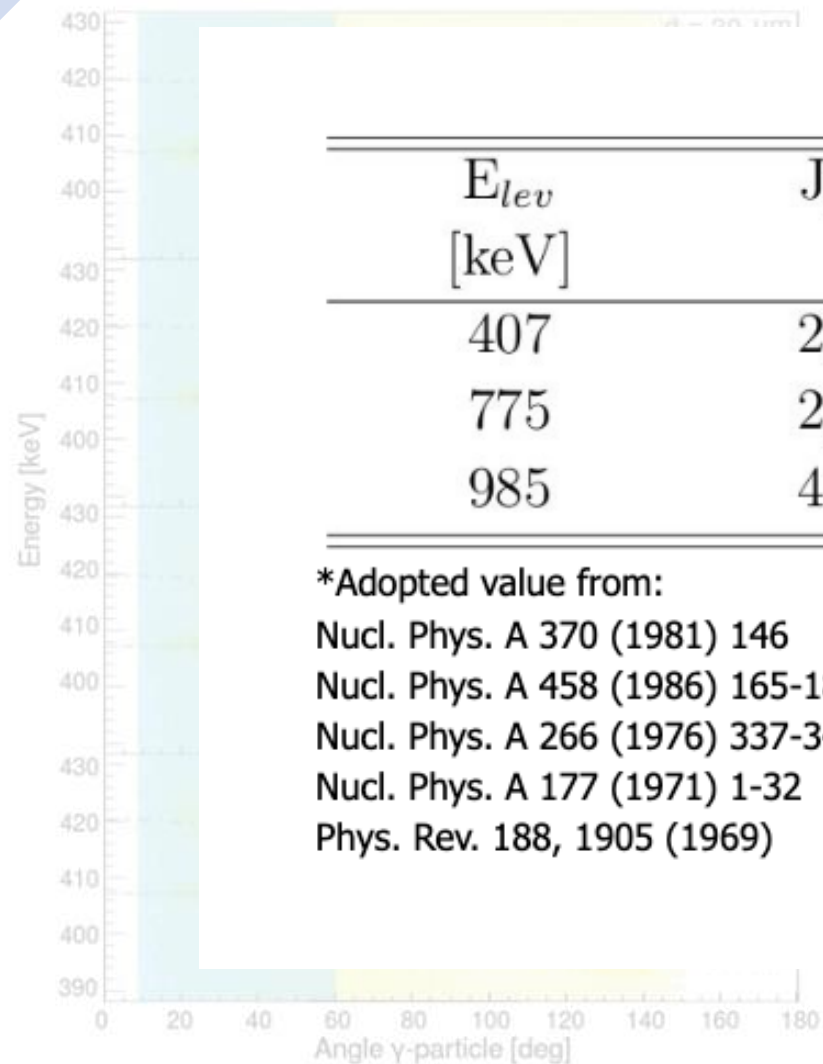


Measured: $t_{1/2} = 19.3(3)$ ps
 Literature: $*t_{1/2} = 22.25(15)$ ps

*Adopted value from:

- Nucl. Phys. A 370 (1981) 146
- Nucl. Phys. A 458 (1986) 165-187
- Nucl. Phys. A 266 (1976) 337-345
- Nucl. Phys. A 177 (1971) 1-32
- Phys. Rev. 188, 1905 (1969)

Lifetime Measurement of the 2_1^+



E_{lev} [keV]	J_i^π	$t_{1/2}^{DDCM}$ [ps]	$t_{1/2}^{Lit}$ [ps]
407	2_1^+	19.3(3)	22.25(15)
775	2_2^+	30.3(4)	27(4)
985	4^+	4.7(4)	3.3(3)

*Adopted value from:
 Nucl. Phys. A 370 (1981) 146
 Nucl. Phys. A 458 (1986) 165-187
 Nucl. Phys. A 266 (1976) 337-345
 Nucl. Phys. A 177 (1971) 1-32
 Phys. Rev. 188, 1905 (1969)

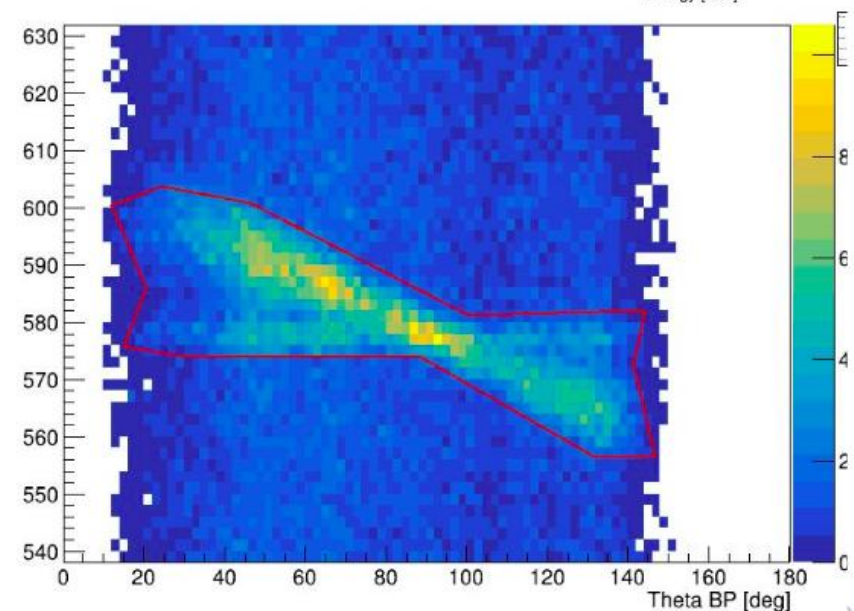
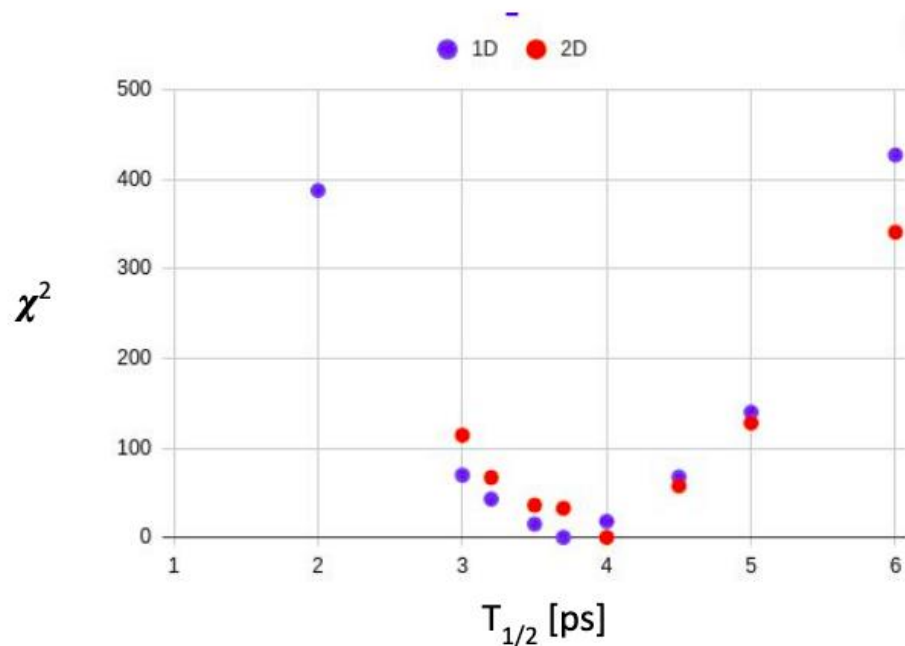
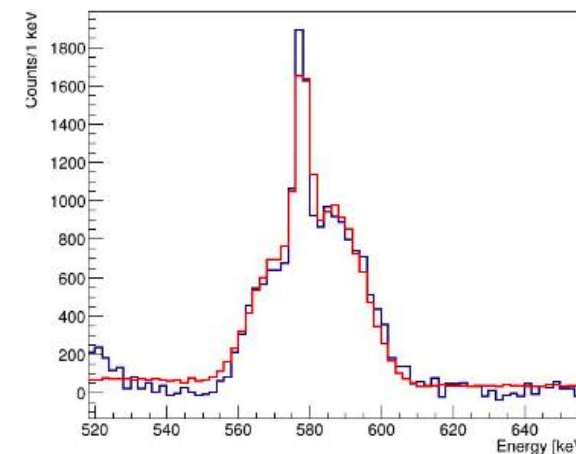


Nucl. Phys. A 177 (1971) 1-32
 Phys. Rev. 188, 1905 (1969)



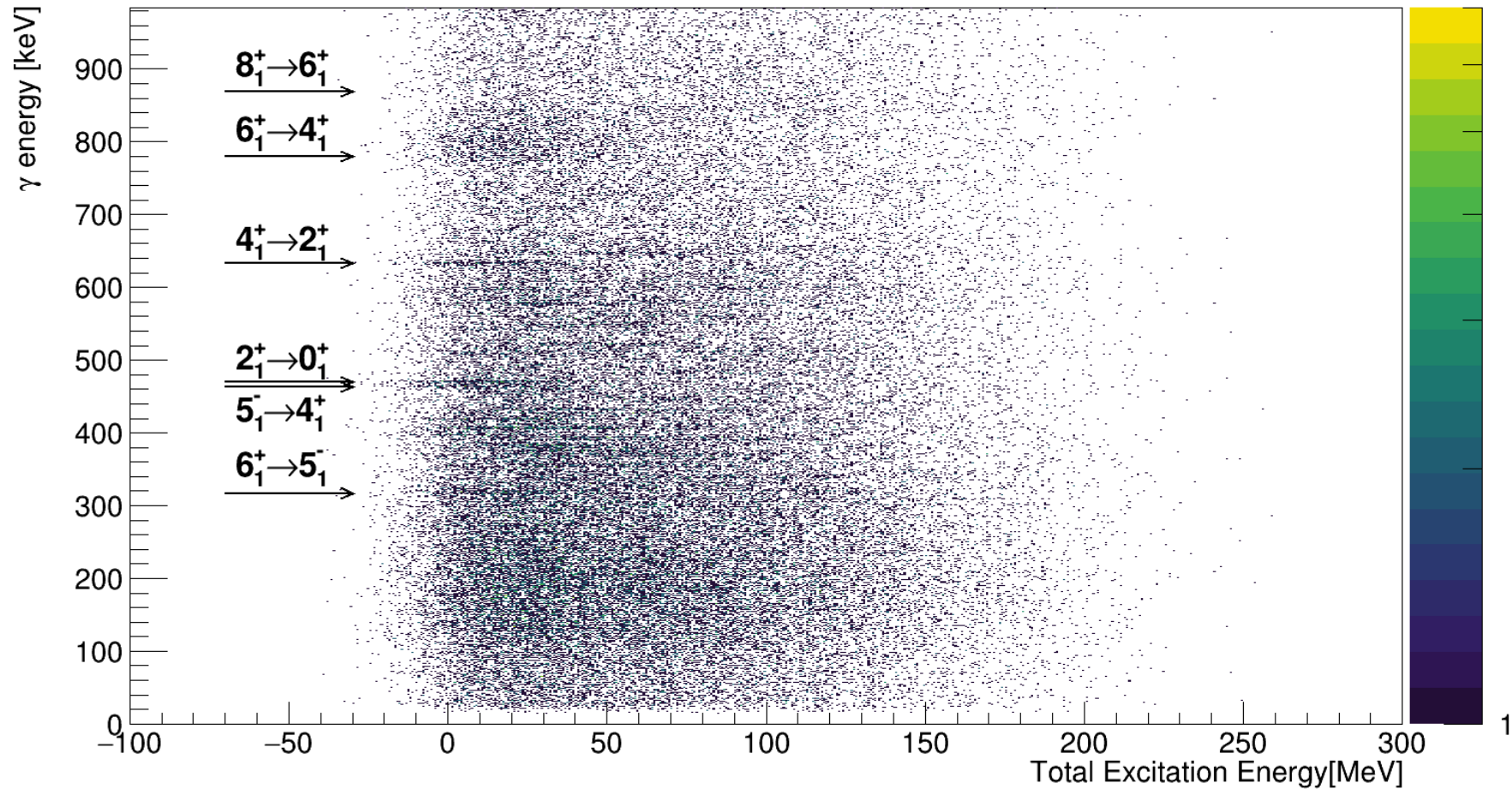
Lifetime Measurement of the 2_1^+

- AGATA simulation package + Geant4
- Two approaches used:
 - 1D - fit the gamma ray spectrum
 - 2D - fit each pixel of the lineshape matrix
- In both cases the simulations reproduce well the known lifetime of the 4^+ state: $T_{1/2} = 3.7$ ps



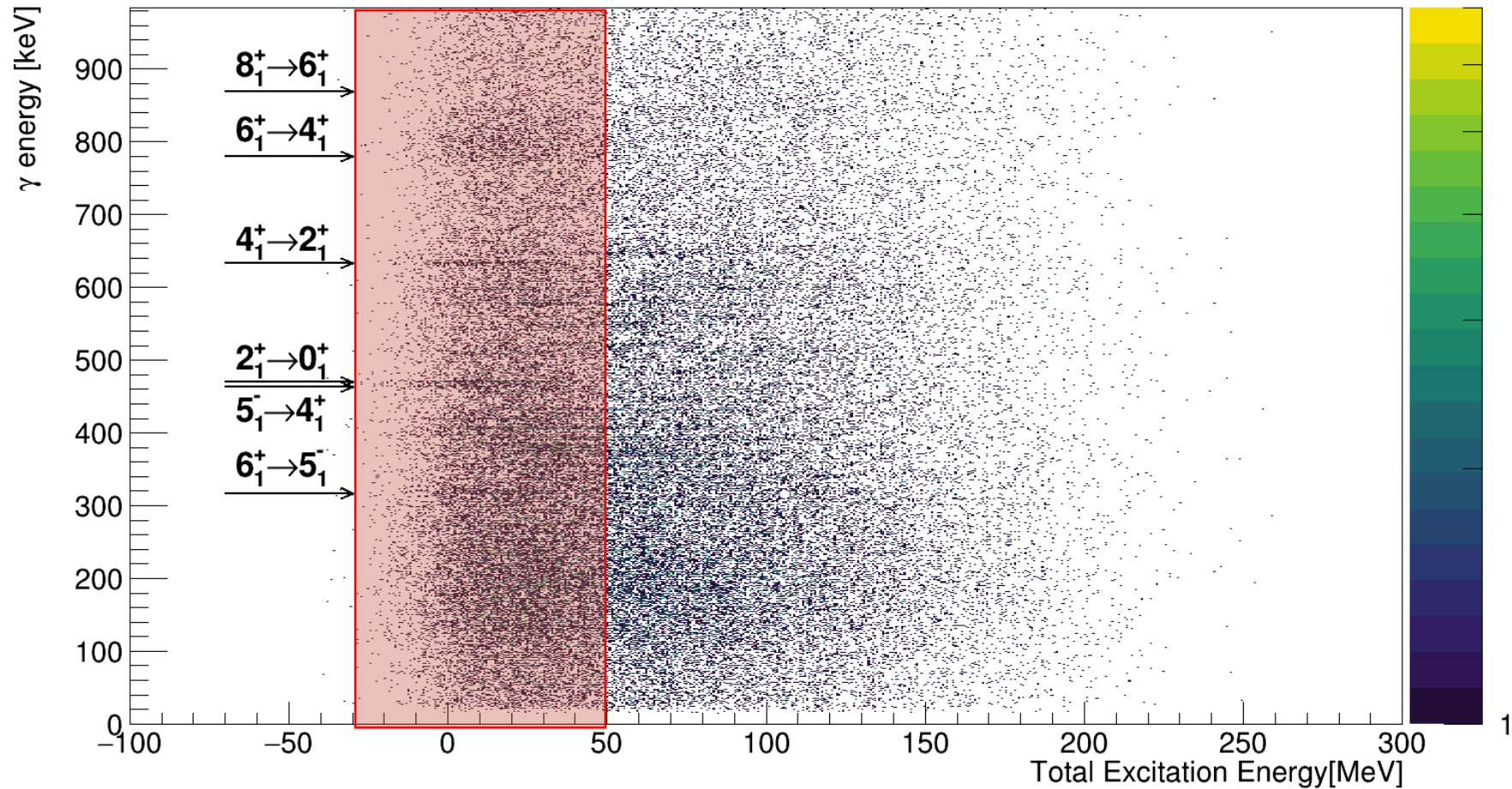


Q-value Analysis: ^{200}Pt

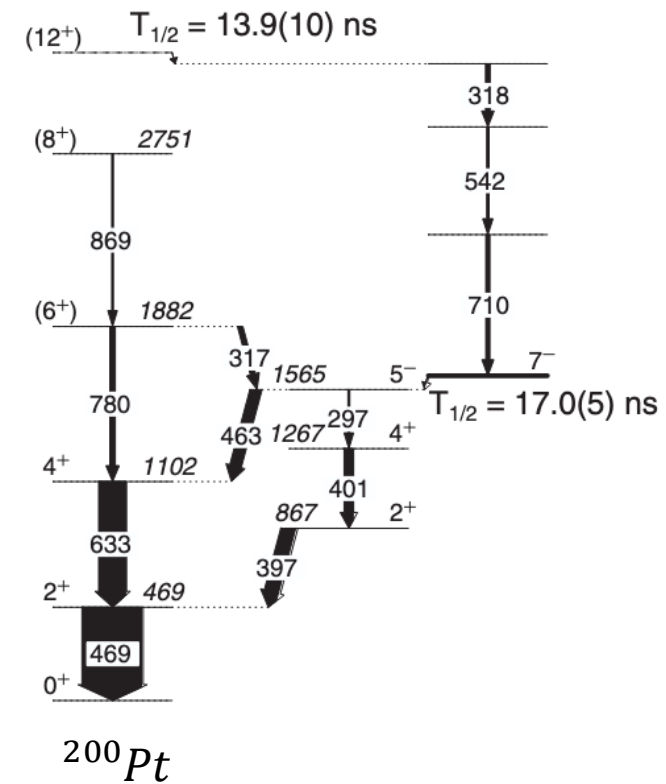
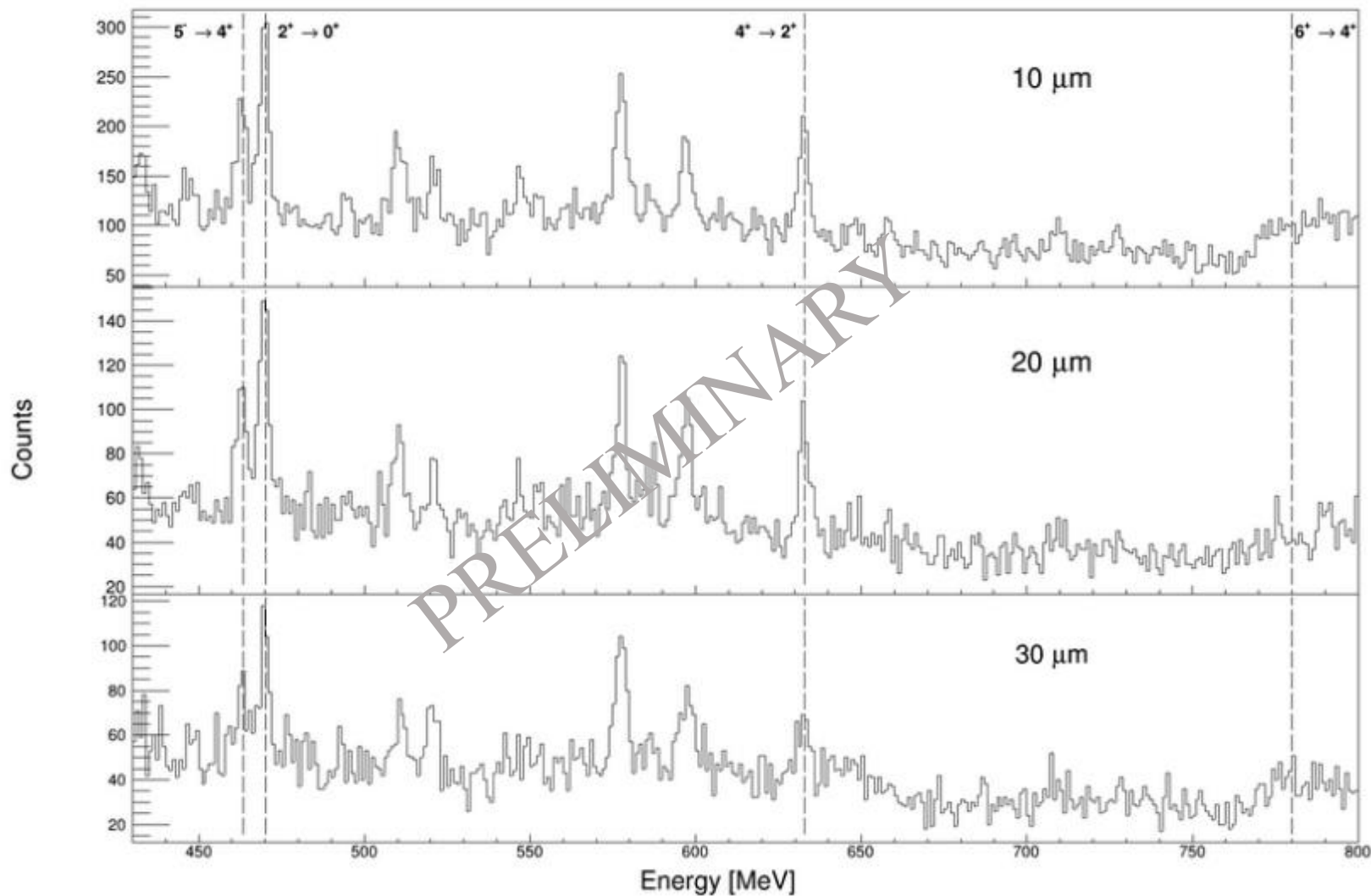




Q-value Analysis: ^{200}Pt



^{200}Pt





Summary and Future Work

- Lifetimes measurements in ^{198}Pt using the reversed plunger configuration: 2_1^+ , 2_2^+ , 4_1^+
- The measured lifetimes are compatible with the literature.

Ongoing...

- Performing a 2D fit of the experimental data employing Geant4 simulations (J. Pellumaj).
- Lifetime measurements in ^{196}Os , ^{200}Pt , and study shape transitions.



Collaboration Members:

D. Brugnara, M. Sedlak, J. Pellumaj, B. Gongora-Servin, J.J. Valiente-Dobón, A. Goasduff,

P. Aguilera, G. Andretta, F. Angelini, M. Balogh, M. Beckers, J. Benito, G. Benzoni, L. Corradi, M. del Fabbro, F. Dunkel, A. Ertoprak, E. Fioretto, F. Galtarossa, A. Giaz, A. Gottardo, A. Gozzelino, C. Lakenbrink, D. Mengoni, G. Montagnoli, R. Nicolás del Álamo, R. Pérez Vidal, S. Pigliapoco, E. Pilotto, M. Poletti, S. Rahaman K. Rezykina, J. Skowronski, A. Stefanini, D. Stramaccioni, S. Szilner, F. Wu, I. Zanon, L. Zago.

Thank you for your attention!

^{200}Pt lifetime measurements @ IFIN-HH

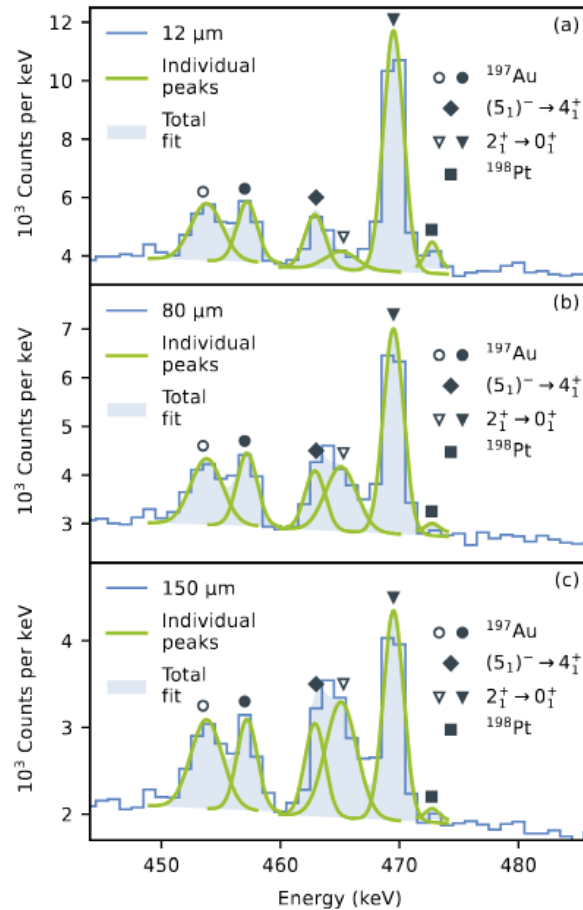


TABLE I. Resulting lifetimes and reduced transition strengths for the $4_1^+ \rightarrow 2_1^+$ and $2_1^+ \rightarrow 0_1^+$ transitions of ^{200}Pt determined in this work.

Transition $J_i \rightarrow J_f$	Lifetime	$B(E2; J_i \rightarrow J_f)$	
	in ps	in $e^2\text{fm}^4$	in W. u.
$2_1^+ \rightarrow 0_1^+$	23.8(11)	1460^{+80}_{-70}	$21.0^{+1.1}_{-1.0}$
$4_1^+ \rightarrow 2_1^+$	2.6(3)	3040^{+430}_{-340}	44^{+7}_{-5}

arXiv:2509.20915 [nucl-ex]

Reversed Plunger Setup

